

**EMIE3D - v2.10**  
**INTEGRAL EQUATIONS ALGORITHM FOR MODELING**  
**MAGNETOTELLURIC AND FINITE SOURCE EM RESPONSES OF**  
**THREE-DIMENSIONAL BODIES IN LAYERED EARTHS**

User Documentation

by

Philip E. Wannamaker

Geophysical Consultant  
3048 South 2850 East  
Salt Lake City, Utah 84109

April, 1995

## TABLE OF CONTENTS

ABSTRACT .....	1
INTRODUCTION .....	2
DOCUMENTATION .....	4
Program Organization.....	4
Input File .....	6
Output Files .....	12
Model Design .....	14
THEORY.....	16
Governing Differential and Integral Equations.....	16
Matrix Formation.....	18
Matrix Green's Functions .....	19
Receiver Green's Functions.....	22
ACKNOWLEDGEMENTS.....	28
REFERENCES .....	29
FIGURES .....	31
APPENDIX.....	32
Sample Inputs and Outputs .....	32

## ABSTRACT

Algorithm EMIE3D-v2.10 is an integral equations program for simulating magnetotelluric (MT), CSAMT, dipole-dipole, and loop-loop (including airborne) EM responses of three-dimensional (3-D) resistivity structure in a layered earth. It has been intended to create a program which can accommodate diverse electromagnetic (EM) sources within a unified input and computational framework. In the integral equations method, inhomogeneous structure is replaced by an equivalent current distribution which is approximated by pulse basis functions. A matrix equation is constructed using the electric tensor Green's function appropriate to the layered earth, and it is solved for the vector current in each cell. Subsequently, scattered fields are found by integrating electric and magnetic tensor Green's functions over the scattering currents. One-dimensional tabulation and interpolation of the Hankel transforms of the tensor Green's functions greatly speeds matrix and receiver field evaluation over direct Hankel transform calculation. Recent progress with the algorithm includes the ability to simulate 3-D structures which outcrop, which transect layer interfaces, and which extend indefinitely in one or more directions. The most important factor in achieving this capability is an accurate treatment of the electric surface charge. In particular, a previous integro-difference formulation for evaluating charges has been abandoned in favor of true surface integrations over the source cells with potential differencing across the field cells in the 3-D body. The new procedure constitutes a good approximation to Galerkin's method while preserving internal consistency in terms of pulse basis functions. Example input and output files showing forward problem results are included at the end of this documentation for user verification.

## INTRODUCTION

EMIE3D-v2.10 is a batch-mode Fortran algorithm for magnetotelluric, CSAMT, dipole-dipole, and loop-loop (including airborne) EM modeling of three-dimensional (3-D) bodies in layered earths. It is based on the theory of integral equations as described in Wannamaker et al. (1984) and Wannamaker (1991), and in the main body of this text. Integral equations are most efficient for modeling one or a few buried prisms and have been valuable for basic physical understanding and for establishing the validity of one- and two-dimensional interpretation of field data. Integral equations are pursued also because satisfactory 3-D differential solutions have been slow to emerge (Hohmann, 1988). While it is generally acknowledged that differential methods should be better-suited for arbitrarily complex 3-D earths, and progress in this area is continuing (e.g., Madden and Mackie, 1989; Mackie et al., 1993), both integral and differential techniques are needed because they have complementary domains of applicability and serve as cross-checks on accuracy for each other. Increased availability of supercomputer facilities also is broadening the class of models that integral equations can accommodate.

It has been intended with EMIE3D to create a program which can accommodate diverse electromagnetic (EM) sources within a unified input and computational framework. Recent innovations in our algorithm include the ability to model structures which outcrop, which transect layer interfaces and which extend indefinitely in one or more dimensions (Figure 1). The principal limitation remaining is the inability to model bodies at very high induction numbers where vortex current flow becomes important (see Newman and Hohmann, 1988). However, the user has the option of simulating structures with no, one, or two vertical planes of symmetry. The program currently runs in batch mode on an IBM-compatible 80486 PC and only minor modifications should be necessary for implementation on other systems. As with any 3-D modeling program, EMIE3D can be demanding of computer resources for all but simple structures. It is recommended that users perform their own convergence tests such as those of Ting and Hohmann (1981) to understand the minimum requirements for discretization of a structure.

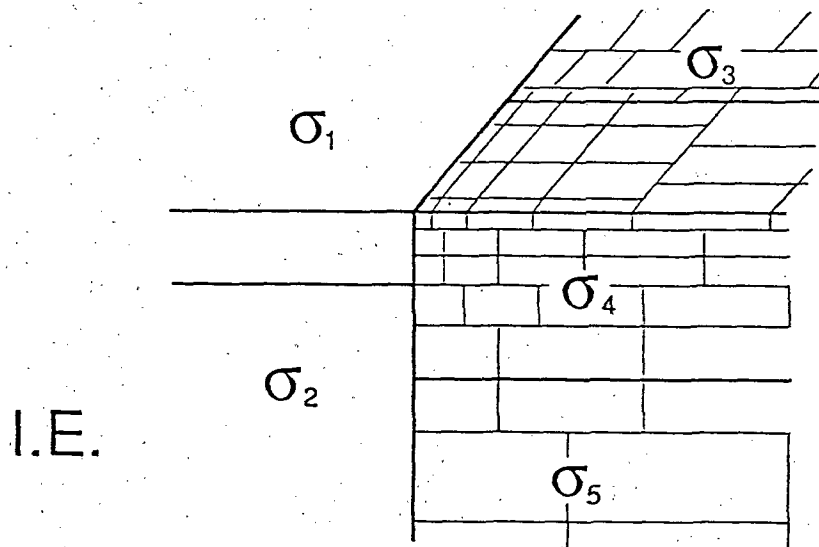
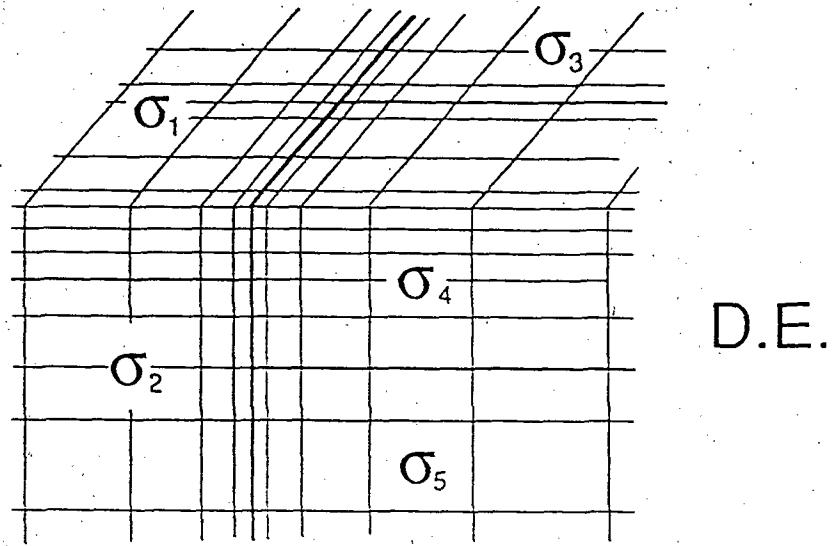


Figure 1. Schematic three-dimensional structure as it would be represented in both differential (D.E.) and integral equation (I.E.) modeling. For the latter,  $\sigma_1$  and  $\sigma_2$  are host layers. The inhomogeneity is composed of media  $\sigma_3$ ,  $\sigma_4$  and  $\sigma_5$  discretized into layers of rectangular cells (pulse basis functions). Away from the central region, the cell dimensions can grow geometricaly in all three dimensions according to the similar fall-off of influence of more distant structure.

## DOCUMENTATION

To begin, the flow of program execution of EMIE3D is summarized below. Details of the procedure may be studied in the Theory section. Subsequently, a list of input and output variables is provided.

### Program Organization

To obtain EM response functions over a 3-D body in a layered host, three primary tasks must be carried out. These are accomplished under the driver EMIE3D in subroutine modules MATCAL, MATSOL, and RCVFLD. The first computes matrix equations defining the vector electric current in the cells making up the discretized 3-D structure. The second program factors and solves the matrices to determine those currents. Finally, RCVFLD computes primary and secondary electric and magnetic fields at the receivers using the primary source and body cell currents. There is also a module of subroutines, EMHANK, which computes EM Hankel transforms, and which must be linked with EMIE3D to run. Unlike earlier versions of the 3-D integral equations code developed by researchers at Utah, EMIE3D is capable of multi-frequency simulations in a single execution. This has made the integral equations evaluations more efficient and paves the way for inversion applications.

Module MATCAL computes one to four matrices describing the electric coupling between the rectangular cells comprising the body for arbitrary polarizations of incident finite-source or plane-wave fields. This computation involves numerous complex numerical integrations proportional to the square of the number of body cells. The primary and secondary Green's functions for the rectangular cells comprising the body have been split into volume and surface contributions with subsequent volume and surface midpoint integrations. The electric charge components of the whole-space, tensor Green's functions also are evaluated using surface charge potential differences (see Theory section). Hankel transforms for the secondary Green's functions obtain

through 1-D cubic interpolation of tabulated values computed in EMHANK. The entire Green's functions only need to be computed once (each frequency) for all matrices, since these matrices differ just in the assembly of these functions according to the group symmetry relations between fields in cells in different quadrants (see Theory section). However, in case the structure being modeled has no planes of symmetry, only one matrix need be computed. With one plane of symmetry, four matrices still are assembled. These matrices are independent of cell conductivity at this point (see Theory section) and may be saved for efficient modeling of structures with the same discretization but different cell conductivities.

Module MATSOL solves the matrices for the electric currents in the rectangular cells using the electric fields incident in the cells in the layered earth as the source vectors. Information about the cell conductivities is added to the matrices just before their solution. The solution is obtained through the method of L-U factorization (Ralston, 1965). A general matrix reduction subroutine is used since the coupling matrices are full. The number of matrices which need to be solved depends on the symmetry of the structure, as stated previously. The factored matrices are saved in separate disk files in case the user wishes to solve for new source vectors subsequently. The matrices are well-conditioned due to the strength of the diagonal self-cell terms and worthwhile future investigations could consider iterative matrix solutions to improve speed and storage.

Module RCVFLD calculates electric and magnetic fields at receiver points from the primary sources and from the scattering currents within the 3-D body. It again involves numerical Green's function integrations, now proportional to the product of cells and receivers. As was the case for construction of the coupling matrices by MATCAL, the tensor Green's functions are separated into volume current and surface charge components, with the latter's electric fields evaluated using potential differences across the receiver bipoles where possible. The Green's functions only need to be computed once for all polarizations of incident field, since they are independent of the source fields. As was the case for the matrices, the cell-receiver

integrations are independent of cell conductivity and may be saved for subsequent models where only the cell properties have changed. Subroutine MTLQS within RCVFLD computes MT quantities from the secondary fields at the receivers. Impedances, apparent resistivities and phases and tipper are calculated in original (x-y) and principal coordinates. Subroutine CSAMTQ computes tensor CSAMT quantities from receiver fields. Quantities are analogous to those for MT. Subroutine DDPQS computes resistivity/IP quantities for the colinear dipole-dipole array. Pseudosections of apparent resistivity and phase may be output. Subroutine CENLUP computes magnetic fields responses for the central loop configuration. Subroutine SLNGRM computes surface, sub-surface, or airborne loop-loop responses for horizontal coplanar (HCP), vertical coaxial (VCA), or vertical coplanar (VCP) configurations.

Module EMHANK computes 1-D tables of electric and magnetic Hankel transforms and transform differences for cubic interpolation by module MATCAL in constructing the matrix equations, by MATSOL in computing primary electric source fields in each cell of the discretized body, and by RCVFLD in computing receiver fields. Hankel transformation in EMHANK is achieved using the filter weights of Anderson (1979) incorporating lagged convolution. The range of horizontal separation ( $r$ ) in the table is set in a data statement and currently is sufficient for the range 0.1 m to 10,000 km. This is presumed to be adequate for all scales of simulation in EM geophysics.

#### Input File

Algorithm EMIE3D requires just one user-input file: INEM3D. It is created using the system editor. Not all variables in INEM3D are used by all three program modules, and output files generated by some of the programs may be used as input files for programs run subsequently. In particular, the body cell current densities solved in module MATSOL reside in unformatted file SCAT. A complete list of input and output files as well as definitions of all input variables appear at the head of each program. All quantities are in MKS units. The following is



a list of the input variables in INEM3D. The variables required are listed as Fortran records, i.e., in groups recognized by individual READ statements.

Record 1: Format - Free

NSTYP - Source type to be modeled

- If .eq. 0, magnetotellurics (MT) modeled
- If .eq. 1, tensor CSAMT with grounded bipole or loop sources modeled
- If .eq. 2, colinear dipole-dipole array modeled
- If .eq. 4, colinear horizontal central loop EM modeled
- If .eq. 6, colinear offset small loop arrays (including airborne and subsurface)

The value NSTYP = 3 is currently reserved for future implementation of another galvanic array (e.g., gradient).

NFREQ - Number of frequencies to be simulated.

NLYR - Number of layers in the 1-D host, including basal half-space

MFCTR - Matrix factorization option.

- If .eq. 0, matrices have already been factored and reside in disk files MTXF#.

They may be read by module MATSOL for reduction of new source vectors.

- If .eq. 1, matrices need to be generated and factored.
- If .eq. 2, matrices have been generated but still need to have cell conductivity information added and to be factored.
- If .eq. 3, matrices have been factored and solved already to yield body currents file 'SCAT'.

Note: Very large matrix disk files (totalling 100 Mbytes or more) may result with MFCTR = 2 for large models and many frequencies. By default, EMIE3D is distributed with files MTXU# and MTXF# overwritten after each frequency. Matrices for all frequencies can be saved and reutilized by enabling the statement incrementing the direct access file record counter (variable NDAMU) just after the call to subroutine MATSOL in EMIE3D.

Record 2: Format - Free

D - Array of layer interface depths (omit if host is a half-space, i.e., NLYR = 1).

RHOL - Array of layer resistivities (real component in ohm-m), including basal half-space.

The next few input records vary according to source, and thus are listed according to value of NSTYP.

For MT modeling (NSTYP = 0):

Record 3: Format - Free

NREC - Number of MT sites (receivers on a given level of z)

NLVZ - Number of levels in z at which receiver fields may be computed.

ZLEN1 - length of E-field receiver bipoles in m (same for x,y,z, components).

NTFQ - Total field quantity option.

- If .eq. 0, compute just receiver field couplings without MT quantities.

- If .eq. 1, compute receiver couplings and MT quantities.

- If .eq. 2, compute MT quantities from existing receiver field couplings in files DCRCC and ACRCC and body currents in SCAT. File ACRCC contains AC and layering Green's functions integrated in a previous run where TFQ = 0 or 1 and which are added to the DC terms in file DCRCC.

- If .eq. 3, compute just layered earth MT quantities at each receiver site.

Record 4: Format - Free

XREC, YREC - Array of horizontal coordinates of receivers

Record 5: Format - Free

ZREC - Array of levels in z at which receiver fields may be computed. ZREC(1) = 0. adequate for surface fields.

For CSAMT modeling (NSTYP = 1):

Record 3: Format - Free

NREC - Number of CSAMT sites (receivers on a given level of z)

NLVZ - Number of levels in z at which receiver fields may be computed.

ZLEN1 - length of E-field receiver bipoles in m (same for x,y,z, components).

NTFQ - Total field quantity option.

- If .eq. 0, compute just receiver field couplings without CSAMT quantities.

- If .eq. 1, compute receiver couplings and CSAMT total-field quantities.

- If .eq. 2, compute CSAMT quantities from existing receiver field couplings in files DCRCC and ACRC and body currents in SCAT.

- If .eq. 3, compute just layered earth CSAMT quantities at each receiver site.

Record 4: Format - Free

XREC,YREC - Array of horizontal coordinates of receivers

Record 5: Format - Free

ZREC - Array of levels in z at which receiver fields may be computed. ZREC(1) = 0. adequate for surface fields.

Record 6: Format - Free

XSRC,YSRC - Array (of two) of locations of centers of bipoles or loops which are sources of CSAMT fields.

Record 7: Format - Free

SLEN,SORI - Array (of two) of lengths (in m) and orientations (in degrees clockwise from +x) of sources.

For dipole-dipole modeling (NSTYP =2):

Record 3: Format - Free

NREC - Number of bipoles in colinear dipole-dipole array. Serves for both sources and receivers in this array.

NIP - Induced Polarization option.

- If .eq. 0, apparent resistivity modeling only

- If .eq. 1, induced polarization modeled too

ZLEN1 - Length of array bipoles in m.

AORI1 - Orientation of colinear array in degrees clockwise from +x axis. For arrays perpendicular to bodies elongate in x-direction, this value would be 90.

NSPC - Maximum N-spacing in dipole-dipole array

NTFQ - Total voltage quantity option.

- If .eq. 0, compute just bipole E-field couplings without dipole-dipole quantities.

- If .eq. 1, compute bipole couplings and dipole-dipole quantities.

- If .eq. 2, compute dipole-dipole quantities from existing bipole couplings in files DCRCC and ACRC and body currents in SCAT.

- If .eq. 3, compute just layered earth dipole-dipole quantities for the array.

Record 4: Format - Free

XMID,YMID - Offset of center of dipole-dipole array from origin of 3-D body in m.

Record 5: Format - Free

RHOLA - Array of layer resistivities (phase angle in mrad), including basal half-space, if

IP is modeled (NIP = 1). READ statement is commented out by default.

For central loop EM modeling (NSTYP = 4):

## Record 3: Format - Free

NSRC - Number of sources in colinear loop EM array.

NREC - Number of receivers per source in colinear loop EM array.

NLVZ - Number of levels of receivers (for downhole application).

ZLEN1 - Separation in m between sources in colinear array.

AORI1 - Orientation of colinear array in degrees clockwise from +x axis. For arrays perpendicular to bodies elongate in x-direction, this value would be 90.

NTFQ - Total field quantity option. Analogous to CSAMT and dipole-dipole cases.

## Record 4: Format - Free

XMID, YMID - Offset of center of loop EM array from origin of 3-D body in m.

## Record 5: Format - Free

XREC, YREC - Array of horizontal coordinates of receivers with respect to loop source.

For offset small loop EM modeling (NSTYP = 6):

## Record 3: Format - Free

NSRC - Number of sources in colinear loop EM array.

NREC - Number of receivers per source in colinear loop EM array (typically 1).

NLVZ - Number of levels of receivers (for downhole application).

ZSPC1 - Data station spacing in m in colinear array.

AORI1 - Orientation of colinear array in degrees clockwise from +x axis. For arrays perpendicular to bodies elongate in x-direction, this value would be 90.

NTFQ - Total field quantity option. Analogous to CSAMT and dipole-dipole cases.

## Record 4: Format - Free

XMID, YMID - Offset of center of loop EM array from origin of 3-D body in m.

ZSRC1 - Depth of loop-loop array (negative for airborne sources). ZSRC1 = 0.  
adequate for surface fields. Multiple receiver depths per source can be specified in the section of subroutine READIN particular to this source module.

LPRFMT - Source-receiver loop format

- If .eq. 1, horizontal coplanar (HCP) array
- If .eq. 2, vertical coaxial (VCA) array
- If .eq. 3, vertical coplanar (VCP) array

Record 5: Format - Free

XREC, YREC - Array of horizontal coordinates of receivers with respect to loop source.

This typically represents source-receiver separation.

The following input variables apply to the 3-D body and are common to all source configurations.

Record 6 (for MT): Format - Free

NRES - Number of different resistivity values in the 3-D body

NCZ - Number of levels of cells in the body

ISYM - If .eq. 0, body has no vertical planes of symmetry

- If .eq. 1, body has one vertical plane of symmetry (x-z)

- If .eq. 2, body has two vertical planes of symmetry

XOB, YOB - Location of body relative to receivers. This value is added to the cell locations in the program to place them w.r.t. the receivers.

- If isym .eq. 0, xob = -x axis limit of body,

yob = -y axis limit of body,

- If isym .eq. 1, xob = -x axis limit of body, yob = 0.

- If isym .eq. 2, xob = 0., yob = 0.

Record 7: Format - Free

R2R - Array of NRES resistivities (real component in ohm-m) in the body.

Record 8: Format - Free

R2RA - Array of NRES resistivities (phase angle in mrad) in the body if IP modeled (NIP = 1).

Record 9: Format - Free

SIZZ - Vertical extent of a given level of cells

DEPC - Depth of a given level of cells

NCX, NCY - Number of cells in x- and y- directions in a given level

Record 10: Format - Free

SIZX - Array of sizes of cells in x-direction in a particular level.

Record 11: Format - Free

SIZY - Array of sizes of cells in y-direction in a particular level.

Record 12: Format - Free

NPT - Integer labels assigning resistivity R2R to a particular cell in a particular level.

### Output Files

Output files of course also vary according to the particular geophysical method being modeled. The principal output file for all methods is called OTEM3D. For MT, its output variables are:

Header information:

NFREQ, NLYR, NREC	=	Number of frequencies, number of layers, number of receivers
FREQA(I)	=	Array of frequencies
D(I)	=	Array of layer interface depths

RHOL(I)	=	Array of layer resistivities, including basal half-space
RHA1D, PHA1D	=	Apparent resistivity and impedance phase of the layered host

For each site:

XREC, YREC, ZREC, FREQ	=	Receiver site location
EXO1-EXO2-EYO1-EYO2	=	Incident electric fields at the surface for first (1) and second (2) polarizations
HXO1-HXO2-HYO1-HYO2	=	Incident magnetic fields at the surface for first (1) and second (2) polarizations
EXS1-EXS2-EYS1-EYS2	=	Secondary horizontal E fields
HXS1-HXS2-HYS1-HYS2	=	Secondary horizontal H fields
EZS1-EZS2-HZS1-HZS2	=	Secondary vertical E and H fields. EZS is zero at surface but may have finite values subsurface.
EXT1-EXT2-EYT1-EYT2	=	Total horizontal E fields
HXT1-HXT2-HYT1-HYT2	=	Total horizontal H fields
HZO1-HZO2-HZT1-HZT2	=	Incident and total vertical magnetic fields at the surface for first and second polarizations. HZO is zero for MT, but included for CSAMT below.
ZXXI-ZXYI-ZYXI-ZYYI	=	Impedance elements in initial coordinates
RXYI-PXYI-RYXI-PYXI	=	Apparent resistivity and phase from off-diagonal impedance elements ZXYI and ZYXI, in initial coordinates. PYXI translated to first quadrant.
RXXI-PXXI-RYYI-PYYI	=	Apparent resistivity and phase from on-diagonal impedance elements ZXXI and ZYYI, in initial coordinates



**RXYSC-PXYSC-RYXSC**

<b>-PYXSC</b>	=	Scalar apparent resistivity and phase in initial coordinates
<b>KZXI-KZYI-TIPH</b>	=	Tipper elements in initial coordinates, plus tipper magnitude
<b>MAG(Z)STRIKE</b>	=	Axis obtained by maximizing $ Z_{xy} $ , $\pm 90^\circ$ added to correspond with MAG(K) strike.
<b>PHZ(Z)STRIKE</b>	=	Axis obtained by maximizing $\phi_{xy}$ , $\pm 90^\circ$ added to correspond with MAG(K) strike.
<b>MAG(K)STRIKE</b>	=	Axis obtained by maximizing $ K_{zy} $
<b>SKEW-ELIP-SKWM-ELPM</b>	=	Complex skew and ellipticity, and their magnitudes ZYKMK for MAG(K) strike
<b>RXYMZ-PXYMZ-RYXMZ</b>		
<b>-PYXMZ</b>	=	Apparent resistivity and phases from ZXYMZ and ZYXMZ for MAG(Z) strike
<b>RXYMK-PXYMK-RYXMK</b>		
<b>-PYXMK</b>	=	Apparent resistivity and phase from ZXYMK and ZYKMK for MAG(K) strike

Detailed format is apparent from the sample files provided. Also, a summary of some of the previous quantities is written to formatted file PFEM3D for user-written plot routines.

For the CSAMT method, output is written very similar in format to the MT output files. Included in the header information of OTEM3D are also the location, size and orientation of the two grounded source bipoles. Not included is the apparent resistivity and phase of the 1-D host, since this would be a function of receiver location for CSAMT when near-field effects become important. For both MT and CSAMT sources, if there are multiple levels of receivers (NLVZ > 1), then a listing of total field components for all levels is appended to OTEM3D.

For the dipole-dipole method, the principal output file contains simply a standard pseudo-section of apparent resistivity in ohm-m and IP effect in mrad.

Output for both loop EM methods commences with header information on frequency and host layering similar to MT. Subsequently, source-receiver locations and fields normalized by the free-space H-fields are output. Specifically, we have, for HCP mode for example,

FREQ	= Frequency in Hz.
XPLT, YPLT, ZPLT	= X-, y-, and z-coordinates of the data plotting point, which is midway between source and receiver loop.
HZSN	= Secondary vertical H-field due to inhomogeneity normalized by free-space field.
HZON	= Primary vertical H-field due to layered host normalized by free-space H-field.
HZTN	= Total vertical H-field normalized by free-space H-field.

Components y and x are output correspondingly for VCA and VCP configurations. For central loop output, absolute source positions and relative receiver positions are given.

### Model Design

Proper model design is essential in obtaining accurate output from this program. This design is still an art which the geophysicist will gain with experience. One is, in effect, attempting to second-guess field behavior in defining discretization. The following guidelines concerning body discretization will serve as guidelines:

1. Body cell dimensions should not change from one cell to the next by more than a factor of two, or by 1.5 for outcropping bodies with E-field receivers directly above.
2. In the vicinity of a change in resistivity of the body, the cell dimensions should be no more than about  $d/2$  ( $d$  = skin depth) in the body or in the medium where the cell resides.
3. No single resistivity medium should be less than 4 cells wide or 3 cells thick to fit galvanic or geometric variations of the field.
4. Horizontal cell dimensions may increase outwards by factors of two away from the region containing the receivers for structures which extend to great distance in one or more directions.
5. Vertical cell dimensions may increase geometrically downward from the air-earth interface by a factor of 1.5 to 2 due to the geometric decay of influence of deeper cells at the receivers.
6. For outcropping structures, best results are obtained over cell body centers or face centers; results over cell corners are not reliable especially near the edges of conductive inhomogeneity.
7. A maximum resistivity contrast of 100 between the structure and its host layering is recommended.

Following these guidelines, typical solution errors for the total E- and H-fields should be on the order of 3-5% except possibly near the edges of outcropping inhomogeneity.

## THEORY

For completeness and to define terms, the method of integral equations is described. The presentation parallels that of Wannamaker et al. (1984) and Wannamaker (1991).

### Governing Differential and Integral Equations

At all points, the electric and magnetic fields  $(\vec{E}, \vec{H})$  as a function of position  $\vec{r}$  and for an  $e^{i\omega t}$  time dependence obey Maxwell's equations

$$-\vec{\nabla} \times \vec{E} = \hat{z} \vec{H} + \vec{M}_i \quad (1)$$

and

$$\vec{\nabla} \times \vec{H} = \vec{J} + \vec{J}_i \quad (2)$$

where  $\vec{J} = \hat{y} \vec{E}$  is the total current density,  $\hat{y} = \sigma + i\omega\epsilon$  is the admittivity and  $\hat{z} = i\omega\mu$  is the impedivity at any point, and  $\vec{J}_i$  and  $\vec{M}_i$  are impressed electric and magnetic source currents. Conductivity, dielectric permittivity and magnetic permeability are  $\sigma$ ,  $\epsilon$  and  $\mu$ . For magneto-telluric modeling,  $\vec{J}_i$  and  $\vec{M}_i$  are zero.

The total fields in any layer are decomposed into an incident set  $(\vec{E}_i, \vec{H}_i)$ , due to  $\vec{J}_i$  and  $\vec{M}_i$ , and a scattered set  $(\vec{E}_s, \vec{H}_s)$ , contributed by the body. Helmholtz equations in layer  $l$  with the body in layer  $j$  can be written

$$(\bar{\nabla}^2 + k_l^2) \vec{E}_i = \left( \frac{1}{\hat{y}_l} \bar{\nabla} \bar{\nabla} \cdot + \hat{z}_l \right) \vec{J}_i + \bar{\nabla} \times \vec{M}_i \quad (3)$$

$$(\bar{\nabla}^2 + k_l^2) \vec{H}_i = \left( \frac{1}{\hat{z}_l} \bar{\nabla} \bar{\nabla} \cdot + \hat{y}_l \right) \vec{M}_i - \bar{\nabla} \times \vec{J}_i \quad (4)$$

$$(\bar{\nabla}^2 + k_l^2)\vec{E}_s = 0 \quad l \neq j \quad , \quad (5)$$

$$(\bar{\nabla}^2 + k_l^2)\vec{H}_s = 0 \quad l \neq j \quad , \quad (6)$$

$$(\bar{\nabla}^2 + k_j^2)\vec{E}_s = \left(\frac{1}{\hat{y}_j} \bar{\nabla} \bar{\nabla} \cdot + \hat{z}_j\right) \vec{J}_s + \bar{\nabla} \times \vec{M}_s \quad l = j \quad , \quad (7)$$

$$(\bar{\nabla}^2 + k_j^2)\vec{H}_s = \left(\frac{1}{\hat{z}_j} \bar{\nabla} \bar{\nabla} \cdot + \hat{y}_j\right) \vec{M}_s - \bar{\nabla} \times \vec{J}_s \quad l = j \quad , \quad (8)$$

in which  $k_l = \sqrt{-\hat{z}_l}$ .  $\hat{y}_l$  is the wavenumber in layer  $l$ . In (7) and (8),  $\vec{J}_s = (\hat{y}_b - \hat{y}_j)\vec{E}_b$  and  $\vec{M}_s = (\hat{z}_b - \hat{z}_j)\vec{H}_b$  are the equivalent scattering currents substituting for the body, while the total fields within the body, as yet unknown, are  $\vec{E}_b$  and  $\vec{H}_b$  (Harrington, 1961). When layer boundaries intersect the body, subscript  $j$  refers to any layer containing a portion of the body. Henceforth we assume that  $\mu_l$  and  $\mu_b$  equal the free space value  $\mu_0$  everywhere and drop  $\vec{M}_s$  from consideration. Furthermore, displacement currents in the earth may be neglected, so that  $\hat{y}_l = \sigma_l$  and  $\hat{y}_b = \sigma_b$  hereafter.

The solutions to (5) through (8) can be expressed by the integral equations

$$\vec{E}_s(\vec{r}) = \int_v G_l^E(\vec{r}; \vec{r}') \cdot \vec{J}_s(\vec{r}') dv' \quad (9)$$

and

$$\vec{H}_s(\vec{r}) = \int_v G_l^H(\vec{r}; \vec{r}') \cdot \vec{J}_s(\vec{r}') dv' \quad (10)$$

The quantities  $G_l^E(\vec{r}; \vec{r}')$  and  $G_l^H(\vec{r}; \vec{r}')$  are  $3 \times 3$  dyadic Green's functions relating a vector field at  $\vec{r}$  in layer  $l$  to a current element at  $\vec{r}'$  in layer  $j$ , including  $l = j$ . These functions are derived in Wannamaker et al. (1984), but modified forms will be discussed here which improve solution accuracy.

### Matrix Formation

Next we describe a simple matrix solution for the unknown electric field within the body using pulse subsectional basis functions (Harrington, 1968). The body is approximated by  $N$  rectangularly prismatic cells, each of arbitrary aspect ratio with the edge dimensions of cell  $n$  being  $\Delta_{xn}$ ,  $\Delta_{yn}$  and  $\Delta_{zn}$ . Over each cell, the body conductivity  $\sigma_b$  and total electric field  $\vec{E}_b$  are presumed constant. Incorporating arbitrary cell aspect ratios substantially increases flexibility in model definition.

In discretized form, the total electric field at the center of cell  $m$  due to all  $N$  cells is approximated by (Hohmann, 1975)

$$\vec{E}_b(\vec{r}_m) = \vec{E}_b(\vec{r}_m) + \sum_{n=1}^N (\sigma_{bn} - \sigma_j) \vec{\Gamma}_l^E(\vec{r}_m; \vec{r}_n) \cdot \vec{E}_b(\vec{r}_n) \quad , \quad (11)$$

including  $n = m$  (van Bladel, 1961). In equation (11), the electric dyadic Green's function for a rectangular prism of current is

$$\vec{\Gamma}_l^E(\vec{r}_m; \vec{r}_n) = \int_{v_n} G_l^E(\vec{r}_m; \vec{r}') dv' \quad . \quad (12)$$

Rearranging (11) and using more concise notation,

$$\sum_{n=1}^N [\vec{\Gamma}_l^E(mn) - \delta_{mn}/(\sigma_{bn} - \sigma_j)] \cdot \vec{J}_{bn} = -\vec{E}_{im} \quad (13)$$

where  $\vec{J}_{bn} = (\sigma_{bn} - \sigma_j) \vec{E}_{bn}$  is electric current in cell  $n$  and where

$$\delta_{mn} = \begin{cases} \vec{\Gamma} & m = n \\ \vec{0} & m \neq n \end{cases} \quad , \quad (14)$$

with  $\bar{\mathbf{I}}$  and  $\bar{\mathbf{O}}$  being the  $3 \times 3$  identity and null dyadics respectively. When written for all  $N$  values of  $m$ , (13) provides the matrix equation

$$[\bar{\mathbf{M}}] \cdot [\bar{\mathbf{J}}_b] = [-\bar{\mathbf{E}}_i] \quad , \quad (15)$$

to be solved for the electric currents within the cells. From these, secondary receiver fields at  $\bar{r}$  about the inhomogeneity are computed using discrete versions of (9) and (10), specifically

$$\vec{\mathbf{E}}_s(\bar{r}) + \sum_{n=1}^N \bar{\Gamma}_l^E(\bar{r}, \bar{r}_n) \cdot \vec{\mathbf{J}}_b(\bar{r}_n) \quad (16)$$

and

$$\vec{\mathbf{H}}_s(\bar{r}) + \sum_{n=1}^N \bar{\Gamma}_l^H(\bar{r}, \bar{r}_n) \cdot \vec{\mathbf{J}}_b(\bar{r}_n) \quad . \quad (17)$$

### Matrix Green's Functions

Calculation of  $G_l^E(\bar{r}; \bar{r}')$  and its integration to yield  $\bar{\Gamma}_l^E(\bar{r}_m; \bar{r}_n)$  comprise a great deal of the effort in an integral equations solution. When a field cell in the body is in the same layer as the source cell during formation of the matrix  $\bar{\mathbf{M}}$ , the Green's function is defined as having a primary or whole space component plus a secondary component (Wannamaker et al., 1984). Specifically,

$$\bar{\Gamma}_l^E(mn) = P\bar{\Gamma}_l^E(mn) + S\bar{\Gamma}_l^E(mn) \quad . \quad (18)$$

The primary component is usually much more important than the secondary component when constructing the matrix because the latter can be viewed, qualitatively, as arising from more distant

image sources due to the air-earth interface and other layering (Bannister, 1986). The primary component also is analytic in form and therefore  $G_l^E(\bar{r};\bar{r}')$  can be integrated accurately over the cell to give  $\tilde{\Gamma}_l^E(\bar{r}_m;\bar{r}_n)$ . Source and field cells in different layers are coupled only by secondary Green's functions; wholespace components cannot be strictly defined (Wannamaker et al., 1984).

Furthermore, both primary and secondary components are split into volume current and free charge contributions pertaining to the  $\hat{z}_0 \vec{J}_s$  and  $(1/\hat{y}_j) \bar{\nabla} \bar{\nabla} \cdot \vec{J}_s$  terms in (7). The free charge portion can be defined as the gradient of a scalar potential  $\phi$  (Hohmann, 1975). Such a splitting allows volume integrations of the current contribution and surface integrations of the charge contribution. Carrying out surface integrations for the secondary charge Green's functions, explained in more detailed below, is an improvement over Wannamaker et al. (1984) who implement volume integrations throughout for the secondary components.

The primary charge Green's function  $\tilde{\Gamma}_l^E(\bar{r}_m;\bar{r}_n)$  is no longer calculated using the integro-difference method (cf. Hohmann, 1988). Instead, true surface integrations over the body source cells are performed with the coupling to the field cells evaluated using potential differences across the field cells. The potential differences provide the average electric fields across the field cells which, together with the pulse nature of the basis functions, constitutes a good approximation to the Galerkin method of matrix definition (Harrington, 1968; Butler and Wilton, 1975). The DC potential differences across the body field cells are computed using the formula of Kellogg (1929, p. 52) for arbitrary rectangular lamina of charge. The AC portions are calculated using midpoint surface integrations with small argument approximations where necessary. In addition, for body cells which outcrop, a DC dipole image term due to the air is removed from the secondary Green's functions defined below and reintegrated over the image surfaces in the manner just described for the whole-space terms.

The volume integrations for both primary and secondary components are carried out in a fashion similar to Wannamaker et al. (1984) except that the midpoint integrations are generalized to allow evaluation of rectangular cells of arbitrary aspect ratio. The number of midpoints used is determined according to the ratio of the minimum cell edge length to the other two edge lengths, up



to a maximum of four midpoints in any direction. A more time-consuming Galerkin integration does not appear important for the volume term because current close to the fieldpoint has less influence than the anomalous volume as a whole, in contrast to the primary charge. This is true for the secondary Green's functions also due to their lesser size.

The secondary surface Green's functions were defined by Wannamaker (1991) according to equation (7) by not carrying out the divergence operation,  $\bar{\nabla} \cdot \vec{J}_s$ , explicitly. To go a step further for EMIE3D, we omit carrying out the gradient operation on the source current as well, and express the Green's functions as

$$S_{G_{xxj}}^E = \frac{1}{4\pi\hat{y}_j} \left\{ \frac{-\partial}{\partial x'} \frac{\partial}{\partial x} S\gamma_{1j}^E + k_j^2 S\gamma_{3j}^E \right\} \quad , \quad (19a)$$

$$S_{G_{yxj}}^E = \frac{1}{4\pi\hat{y}_j} \left\{ \frac{-\partial}{\partial x'} \frac{\partial}{\partial y} S\gamma_{1j}^E \right\} \quad , \quad (19b)$$

$$S_{G_{zxx}}^E = \frac{-1}{4\pi\hat{y}_j} \left\{ \frac{\partial}{\partial x'} [S\gamma_{4j}^E] \right\} \quad , \quad (19c)$$

$$S_{G_{xyj}}^E = \frac{1}{4\pi\hat{y}_j} \left\{ \frac{\partial}{\partial y'} \frac{\partial}{\partial x} S\gamma_{1j}^E \right\} \quad , \quad (19d)$$

$$S_{G_{yyj}}^E = \frac{1}{4\pi\hat{y}_j} \left\{ \frac{\partial}{\partial y'} \frac{\partial}{\partial y} S\gamma_{1j}^E + k_j^2 S\gamma_{3j}^E \right\} \quad , \quad (19e)$$

$$S_{G_{zyj}}^E = \frac{-1}{4\pi\hat{y}_j} \left\{ \frac{\partial}{\partial y'} [S\gamma_{4j}^E] \right\} \quad , \quad (19f)$$

$$S_{G_{xzz}}^E = \frac{-1}{4\pi\hat{y}_j} \left\{ \left[ \frac{(x-x')}{r} \right] S\gamma_{6j}^E \right\} \quad , \quad (19g)$$

$$S_{G_{yzj}}^E = \frac{-1}{4\pi\hat{y}_j} \left\{ \left[ \frac{(y-y')}{r} \right] S_{\gamma_{6j}}^E \right\} \quad (19h)$$

and

$$S_{G_{zzj}}^E = \frac{1}{4\pi\hat{y}_j} \{ S_{\gamma_{5j}}^E \} \quad (19i)$$

Time-saving and more accurate surface integrations are now possible, using midpoint evaluations also. The Hankel transforms in equation (19) are identical to those given by Wannamaker et al. (1984) with the exception of  $S_{\gamma_{1j}}^E$  and  $S_{\gamma_{4j}}^E$ . For them, the kernels are still identical but the integrand is now  $J_0(\lambda r)/\lambda$  rather than  $J_1(\lambda r)$ . Note that there is no  $S_{\gamma_{2j}}^E$  in (19). Integrating a function which itself is expressed as a divergence is equivalent to evaluating the argument of that divergence at the endpoints of the interval of integration, i.e., over the surface of the source cell. Also, integrating the gradient of a function over an interval is equivalent to evaluating the function at the endpoints of the interval, i.e., a potential difference along the receiver bipole. When the field cell  $m$  and source cell  $n$  reside in different layers, then separating the secondary Green's functions into charge and current contributions and using potential differences appears sufficient to obtain accurate coupling between cells separated by layer interfaces. Potential differencing is also used wherever possible to define the source vector  $\vec{E}_i$  in equation (15). This provides values which are closer to average electric fields over the cells compared to E-field evaluations at the cell centers, which in turn provides a closer approximation to the Galerkin method of source vector definition.

### Receiver Green's Functions

The quantities  $\tilde{\Gamma}_j^E(\vec{r}; \vec{r}_n)$  and  $\tilde{\Gamma}_j^H(\vec{r}; \vec{r}_n)$  in (16) and (17) for the fields at the receivers come about in a similar fashion. When the field point resides in the same layer as a source cell, primary and secondary components to both electric and magnetic Green's functions arise again. However,

in contrast to Wannamaker (1991), the electric field due to the surface charge on the source cell is calculated by potential differencing as was done previously for the matrix. These formulas are applied also to the DC component of the first reflection due to any layer interface immediately below or above the source cell, including the air-earth interface. If field points and source cells are separated by a single layer interface, the DC component of the direct transmission across the interface is evaluated also using the lamina formulas. The remaining AC and secondary charge contributions are computed using midpoint surface integrations as described previously in forming the matrix. The volume current components of the electric and magnetic fields are calculated similarly using volume midpoint integrations. Experience so far has shown that good results over shallow or outcropping bodies can be obtained at cell body centers or face centers. Results near cell corners are not reliable due to unstable behavior of the electric field at the corners of the rectangular lamina.

The form of the secondary electric Green's functions for the receiver fields is identical to equation (19). That of the secondary magnetic Green's functions is given below:

$$S_{G_{xxj}}^H = \frac{1}{4\pi} \left\{ \frac{\partial}{\partial x'} \left[ \frac{(y-y')}{r} \right] S_{\gamma_{1j}}^H \right\} , \quad (20a)$$

$$S_{G_{yxj}}^H = \frac{1}{4\pi} \left\{ \frac{\partial}{\partial x'} \left[ \frac{(x-x')}{r} \right] S_{\gamma_{1j}}^H + S_{\gamma_{3j}}^H \right\} , \quad (20b)$$

$$S_{G_{zsj}}^H = \frac{1}{4\pi} \left\{ \frac{\partial}{\partial y'} S_{\gamma_{4j}}^H \right\} , \quad (20c)$$

$$S_{G_{xyj}}^H = \frac{1}{4\pi} \left\{ \frac{\partial}{\partial y'} \left[ \frac{(y-y')}{r} \right] S_{\gamma_{1j}}^H - S_{\gamma_{3j}}^H \right\} , \quad (20d)$$

$$S_{G_{yyj}}^H = \frac{-1}{4\pi} \left\{ \frac{\partial}{\partial y'} \left[ \frac{(x-x')}{r} \right] S_{\gamma_{1j}}^H \right\} , \quad (20e)$$

$$S_{G_{zyj}}^H = \frac{-1}{4\pi} \left\{ \frac{\partial}{\partial x'} [S_{\gamma_{4j}}^H] \right\} \quad , \quad (20f)$$

$$S_{G_{xzj}}^H = \frac{-1}{4\pi} \left\{ \left[ \frac{(y-y')}{r} \right] S_{\gamma_{5j}}^H \right\} \quad , \quad (20g)$$

$$S_{G_{yzj}}^H = \frac{1}{4\pi} \left\{ \left[ \frac{(x-x')}{r} \right] S_{\gamma_{5j}}^H \right\} \quad , \quad (20h)$$

and

$$S_{G_{zzj}}^H = 0 \quad . \quad (20i)$$

Again, all the Hankel transforms in (20) are identical to those in Wannamaker et al. (1984) with the exception of  $S_{\gamma_{4j}}^H$  whose integrand is  $J_0(\lambda r)/\lambda$  instead of  $J_1(\lambda r)$ . Divergence components of the magnetic Green's functions are only evaluated for grounded bipole sources; they would be omitted for closed-loop current sources.

Finally, the Hankel transforms of both (19) and (20) are calculated through four-point cubic interpolation from tables formed previously. The table values are computed using the filter weights of Anderson (1979) incorporating lagged convolution. Now, the interpolation is just one-dimensional over tables for each pair of field cell/point - source cell depth values  $(z, z')$ . This improved speed of matrix calculation by more than a factor of three over the 3-D cubic interpolation of Wannamaker et al. (1984) and large improvements occurred in the speed of receiver field computation also. In generating the matrix  $\bar{\bar{M}}$ , approximately one-half of the computer time is spent on the DC wholespace surface charge components to the total Green's function integration for  $\bar{\Gamma}_l^E(\bar{r}_m; \bar{r}_n)$ . Formation of the matrix still requires far more time than solving it for most models, and the difficulty of vectorizing the former complicated step makes this problem especially acute on vector machines like the SDSC CRAY YM-P. The integral equation matrix  $\bar{\bar{M}}$  of (15) is full and

we use a general, direct solution to solve it (Ralston, 1965). Implementation of an iterative matrix solution (e.g., Jacobs, 1986; Papadrakakis and Dracopoulos, 1991; Freund, 1992) may become attractive to mitigate storage limitations for very large models. Such iterative schemes are facilitated by formulating the coupling matrix in terms of currents, which makes  $\bar{M}$  symmetric (Xiong, 1992).

Substantial savings in matrix computation time have been achieved with additional programming efforts. For example, a separation of the DC component of the Green's functions for use in calculations at different frequencies has approximately halved matrix formation time, as indicated above. Moreover, for fixed body geometries and host resistivities, large savings are effected by decomposing the coupling matrix  $\bar{M}$  of equation (15) as

$$[\bar{M}] = [\bar{\Gamma} - \Delta \bar{\sigma}^{-1}] \quad (21)$$

where  $\Delta \bar{\sigma}$  is a diagonal matrix of the body cell conductivity differences,  $\bar{\Gamma}$  is a full matrix of cell Green's functions (i.e., equation (12)), and  $\bar{I}$  is the identity matrix. The matrix  $\bar{\Gamma}$  is independent of body cell conductivities and is a function solely of cell geometries and host layering. In iterative forward modeling or inversion of data for example, where cell conductivities are estimated for a fixed ensemble of cells,  $\bar{\Gamma}$  may be saved for each frequency after the first iteration and  $\bar{M}$  updated by simple diagonal matrix subtraction. Where applicable, time savings of one to two orders of magnitude may be possible. Module MATCAL actually computes  $\bar{\Gamma}$ , while  $\Delta \bar{\sigma}^{-1}$  for the particular model or iteration is subtracted in MATSOL. One notes that the body-receiver couplings of equations (16) and (17) are also independent of cell conductivity, and are also saved for subsequent iterations by module RCVFLD.

Computational savings are also made for 3-D bodies with one or two vertical symmetry planes using group theory (Tripp and Hohmann, 1984). For a body with two symmetry planes, the four irreducible representations (symmetry groups) of current flow in the four quadrants of the body are depicted in Figure 2. The group numbers correspond to coding in EMIE3D. Note that the coordinate and quadrant numbering convention here differs from that of Tripp and Hohmann

(1984). Each entry of the four block matrices defining the irreducible representations is given by the summation

$$\Gamma_{ib}^m = \frac{1}{ns} \sum_{k=1}^{ns} s_i(k) \cdot \Gamma_{ik}^m \quad (22)$$

where  $m$  is the representation number,  $k$  is the quadrant number,  $s_i(k)$  is the sign of the particular current component  $J_{ik}^m$  ( $i = x, y, z$ ) in the receiver cell of quadrant  $k$  relative to the sign in quadrant 1

(Figure 2), and  $ns$  is the number of representations for the particular structure ( $ns = 1$  for zero symmetry,  $ns = 2$  for one plane, and  $ns = 4$  for two planes). The term  $\Gamma_{ik}^m$  in (22) is the Green's

function which couples current component  $i$  in a receiver cell in quadrant 1 to any current component  $J_x, J_y, J_z$  in a source cell in quadrant  $k$ . The incident E-fields in each cell of the body are summed similarly to give the source vectors for each irreducible representation. Once the block matrices have been solved for the current representations, the total current in each quadrant  $k$  is the summation

$$J_{ib}^k = \frac{1}{ns} \sum_{m=1}^{ns} J_{ik}^m \quad (23)$$

This summation is carried out in module RCVFLD in computing the receiver fields. For structures

with one symmetry plane (x-z), ~~only groups 1 and 2 are pertinent.~~ *all four symmetry groups still must be defined and solved because the source fields in general are not symmetric about the x-z plane.*

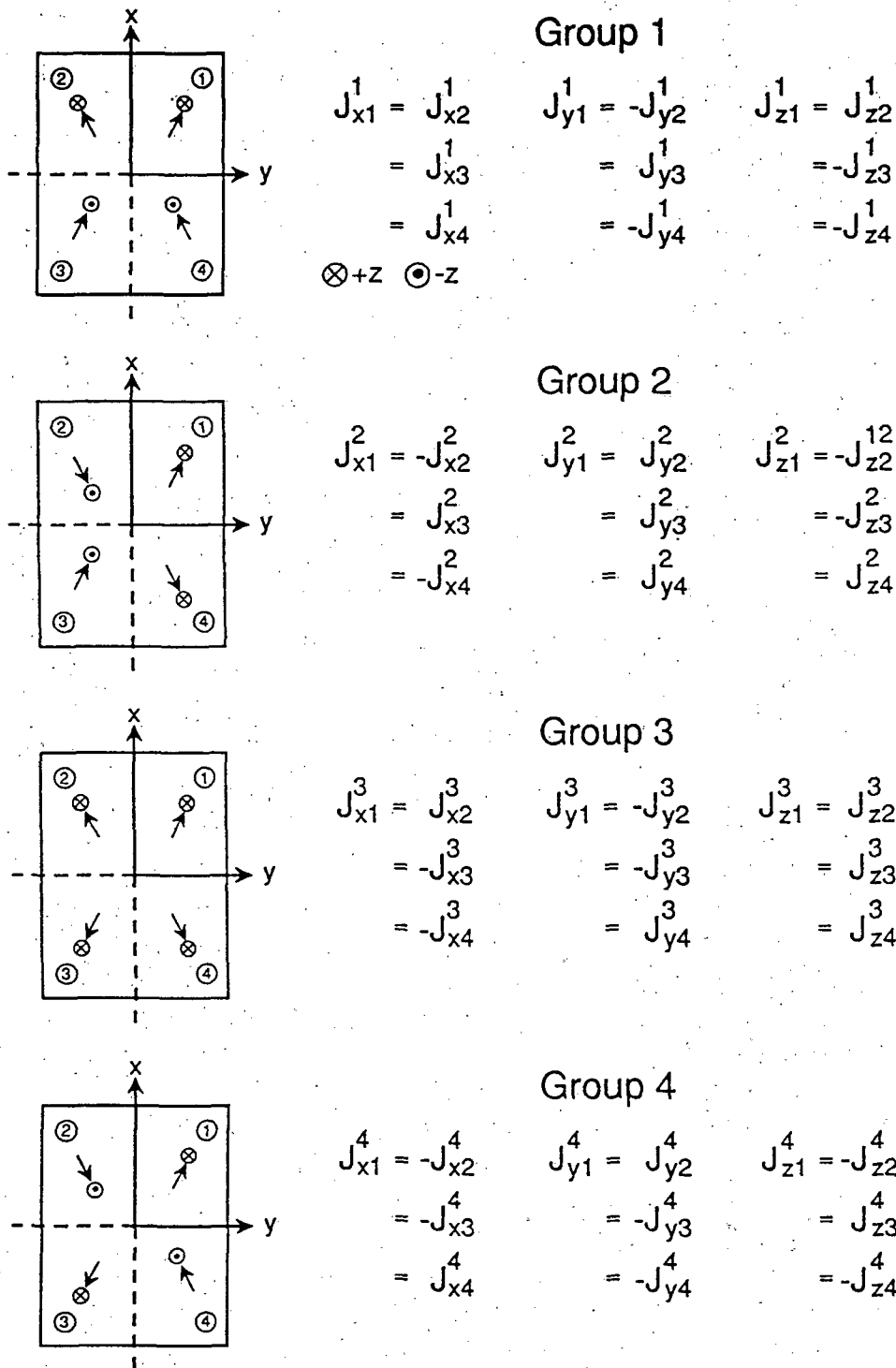


Figure 2. Irreducible representations of body currents for a structure with two vertical planes of symmetry. Groups are numbered as coded in EMIE3D. Arrows show directions of horizontal component of current flow in each quadrant relative to that in quadrant 1, which has positive x and y components. Sign of the z component is indicated according to key with group 1. Quadrant numbers are labeled with circled numbers in the distal corners of each quadrant. For current components, superscript is group number and second subscript is quadrant number.

## ACKNOWLEDGEMENTS

Early stages of this algorithm development were supported under NSF Grants EAR-85000248 and EAR-8708382, Department of Energy contracts DE-AC07-85ID12489, DE-AC07-90ID12929 and DE-FG02-89ER14083. Development also was carried out while the author was a Green Foundation Scholar at the Institute for Geophysics and Planetary Physics, Scripps Institution of Oceanography. Implementation of finite source capability for dipole-dipole and CSAMT methods was supported by Department of Energy contract DE-AC07-90ID12929 and grant DE-FG02-89ER14083, and by the Consortium for Electromagnetic Modeling and Inversion (CEMI) of the University of Utah. Loop-loop EM capability was supported by (CEMI). Numerous informative discussions were held with G. W. Hohmann.



## REFERENCES

- Anderson, W. L., 1979, Numerical integration of related Hankel transforms of orders 0 and 1 by adaptive digital filtering: *Geophysics*, 44, 1287-1305.
- Bannister, P. R., 1986, Application of complex image theory: *Radio Sci.*, 21, 605-616.
- Butler, C. M., and Wilton, D. R., 1975, Analysis of various numerical techniques applied to thin-wire scatterers: *IEEE Trans. Ant. Prop.*, AP-23, 534-540.
- Freund, R.W., 1992, Conjugate gradient-type methods for linear systems with complex symmetric coefficient matrices: *SIAM J. Sci. Stat. Comput.*, 13, 425-448.
- Harrington, R. F., 1961, Time-harmonic electromagnetic fields, McGraw-Hill Electrical and Electronic Engineering Series, New York, 480 p.
- Harrington, R. F., 1968, Field computation by moment methods: reprint edition, Krieger Publ. Co., Malabar, FLA, 229 p.
- Hohmann, G.W., 1975, Three-dimensional induced polarization and electromagnetic modeling: *Geophysics*, 40, 309-324.
- Hohmann, G.W., 1988, Numerical modeling for electromagnetic methods of geophysics, in *Electromagnetic methods in applied geophysics*, ed. by M. N. Nabighian, Society of Exploration Geophysicists, Tulsa, 313-363.
- Jacobs, D. A., 1986, A generalization of the conjugate-gradient method to solve complex systems: *IMA J. Numer. Anal.*, 6, 447-452.
- Kellogg, O. D., 1929, Foundations of potential theory: Dover Publ., New York, 384 p.
- Mackie, R.L., Madden, T.R., and Wannamaker, P.E., 1993, Three-dimensional magnetotelluric modeling using difference equations-part I: theory and comparisons to integral equations solutions: *Geophysics*, 58, 215-226.
- Madden, T. R., and Mackie, R. L., 1989, Three-dimensional magnetotelluric modeling and inversion: *Proc. IEEE*, 77, 318-333.
- Millett, F.B., Jr., 1967, Electromagnetic coupling of collinear dipoles on a uniform half-space, in *Mining Geophysics*, v. II, Soc. Explor. Geophys., Tulsa, Okla., 401-422.
- Newman, G.A., and Hohmann, G.W., 1988, Transient electromagnetic responses of high-contrast prisms in a layered earth: *Geophysics*, 53, 691-706.
- Papadarakakis, M., and Dracopoulos, M.C., 1991, Improving the efficiency of incomplete Choleski preconditionings: *Comm. Appl. Num. Methods*, 7, 603-612.

- Ralston, A., 1965, A first course in numerical analysis: New York, McGraw-Hill Book Co.
- Spies, B. R., and Frischknecht, 1991, Electromagnetic sounding, *in* Electromagnetic methods in applied geophysics, v. 2, ed. by M. N. Nabighian, Society of Exploration Geophysicists, Tulsa, 285-425.
- Tripp, A.C., and Hohmann, G.W., 1984, Block diagonalization of the electromagnetic impedance matrix of a symmetric buried body using group theory: *IEEE Trans. Geosci. and Rem. Sens.*, GE-22, 62-68.
- Van Bladel, J., 1961, Some remarks on Green's dyadic for infinite space: *IRE Trans. Ant. Prop.*, 9, 563-566.
- Wannamaker, P.E., 1991, Advances in three-dimensional magnetotelluric modeling using integral equations: *Geophysics*, 56, 1716-1728.
- Wannamaker, P.E., 1992, IP2DI-v1.00: Finite element program for dipole-dipole resistivity /IP forward modeling and parameterized inversion of two-dimensional earth resistivity structure: University of Utah Research Institute rep. ESL-92002-TR, 62 p.
- Wannamaker, P. E., Hohmann, G. W., and San Filippo, W. A., 1984a, Electromagnetic modeling of three dimensional bodies in layered earths using integral equations: *Geophysics*, 49, 60-74.
- Xiong, Z., 1992, Symmetry properties of the scattering matrix in three-dimensional electromagnetic modeling using the integral equation method: *Geophysics*, 57, 1199-1202.

## FIGURES

1. Schematic three-dimensional structure as it would be represented in both differential (D.E.) and integral equation (I.E.) modeling. For the latter,  $\sigma_1$  and  $\sigma_2$  are host layers. The inhomogeneity is composed of media  $\sigma_3$ ,  $\sigma_4$  and  $\sigma_5$  discretized into layers of rectangular cells (pulse basis functions). Away from the central region, the cell dimensions can grow geometrically in all three dimensions according to the similar fall-off of influence of more distant structure.

2. Irreducible representations of body currents for a structure with two vertical planes of symmetry. Groups are numbered as coded in EMIE3D. Arrows show directions of horizontal component of current flow in each quadrant relative to that in quadrant 1, which has positive x and y components. Sign of the z component is indicated according to key with group 1. Quadrant numbers are labeled with circled numbers in the distal corners of each quadrant. For current components, superscript is group number and second subscript is quadrant number.

A-1. Buried conductive (1 ohm-m) and resistive (100 ohm-m) elongate prisms in a three layer host. The structure has one vertical symmetry plane (x-z) on each side of which there are 80 cells.

A-2. Offset conductive (3 ohm-m) prism model in a resistive (100 ohm-m) host used to demonstrate tensor CSAMT calculations for a body with no planes of symmetry. There are 58 cells in this body. Results are compared to those for purely plane-wave excitation.

A-3. Buried conductive (10 ohm-m) elongate prism in a resistive half-space host (100 ohm-m). The structure has two symmetry planes with 64 cells per quadrant and is simulated for the dipole-dipole resistivity/IP array. Results are compared to those of the UURI 2-D finite element program, IP2DI-v1.00, and to coupling values in Millett's tables.

A-4. Buried low-resistivity (10 ohm-m) layer constructed as an inhomogeneity in a 100 ohm-m half-space. The structure has two symmetry planes with 124 cells per quadrant and is simulated for the central loop configuration with a magnetic field receiver at the center. Cells double in horizontal dimension outward from the center of the loop to the edge of the 3-D body at x and y =  $\pm 4250$  m, and thicken with distance also to economize on cell number. Results are compared to primary fields computed over a three-layer earth, with layer two the same as the 10 ohm-m 'layer' inhomogeneity, using program EMIE3D.

A-5. Buried conductive prism (1. ohm-m) in a resistive half-space simulated for airborne loop-loop arrays. The structure has two planes of symmetry with 24 cells per quadrant. Two loop modes, HCP and VCA, at a height of 30 meters are considered. Secondary and total vertical magnetic fields normalized by the free-space results are computed every 25 m across the center of the prism for a frequency of 1000 Hz.

## APPENDIX

Sample Inputs and Outputs

The modeling program EMIE3D is exemplified using several resistivity structures, one for each source type. Figure A-1 is a body simulated for magnetotellurics and is a buried version of the two-prism model considered by Wannamaker (1991). It is a moderately large model containing 80 cells per half and is used to show a run with one plane of symmetry. The x- and y-axes in the figure define the origin for the receivers, of which there are five along the +y direction (see input file). The body is placed with respect to this origin by the value of  $x_{ob} = -20$  km, which is the negative x-axis limit of the structure. This model was run on an IBM-compatible PC-486/66 with a local bus disk controller, using Lahey EM/32-v5.00 Fortran, and required about 110 s CPU time to form the matrix, 50 s to solve, and 25 s to obtain the receiver quantities.

Figure A-2 is an offset, conductive prism used to demonstrate tensor CSAMT calculations. It is defined in the input file to have zero planes of symmetry to exemplify this option. Note that  $x_{ob} = -1000$  m and  $y_{ob} = -500$  m. Two output files are included here, one for crossed source bipoles at  $x = 0$  m,  $y = -30$  km, and one for separated bipoles at  $x = \pm 15$  km,  $y = -30$  km. The bipole orientation for the second run is more arbitrary also. The model is in the far-field zone of the sources and may be compared to the output for this model for true MT simulation. One sees agreement between both CSAMT results and the MT results within a few percent for apparent resistivity and one degree for impedance phase. On the PC-486/66, the CSAMT results for each model required about 40 s CPU time to form the matrix, 15 s to solve, and 6 s to obtain the receiver quantities.

Figure A-3 is an elongate conductive prism with two planes of symmetry run for the colinear dipole-dipole, resistivity/IP problem. It has been made elongate for comparison to results computed by program IP2DI-v1.00, the UURI finite element algorithm for analogous responses of 2-D structures (Wannamaker, 1992). Thus, a very low frequency of  $f=0.0001$  Hz has been used

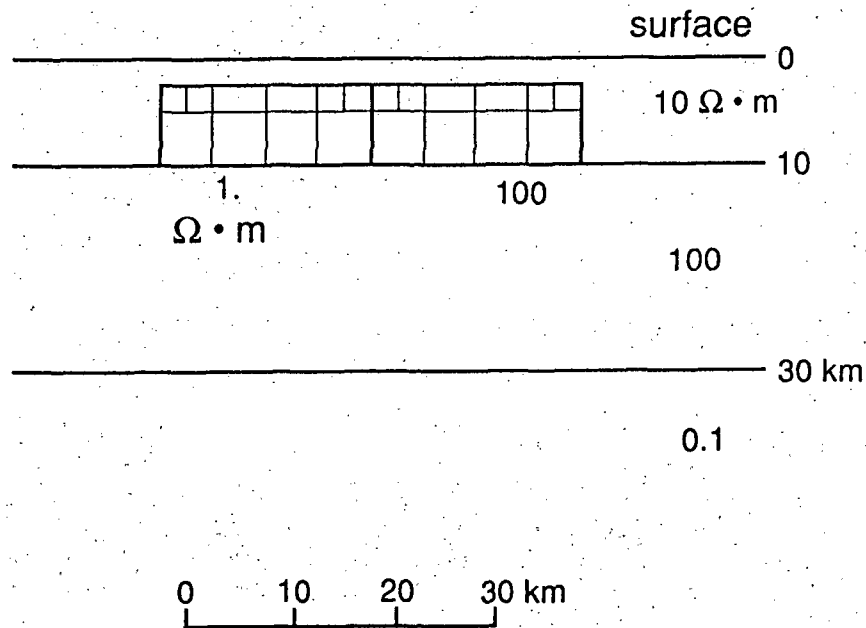
to prevent any EM coupling in the 3-D simulation. In the 3-D body, there are 64 cells per quadrant which grow geometrically in length from the origin. Note that  $x_{ob}$  and  $y_{ob}$  are zero for a body with no symmetry planes. On the PC-486/66, this model required 135 s to form the matrix, 80 s to solve, and 35 s to form the receiver bipole voltages and output. Agreement appears to be within several percent for apparent resistivity, and perhaps somewhat worse for IP effect, but agreement improves substantially with increased discretization of the 3-D body. Moreover, the IP effect from program IP2DI is computed using apparent resistivity Jacobians, which may give an over-estimate by several percent or more, at least for confined bodies. Following these calculations, we verify the AC portion of the code by computing EM coupling phase angle for two values of induction number ( $\theta = 0.05$  and  $0.25$ ) for a uniform half-space and comparing them to those in the tables of Millett (1967). Agreement can be seen to be exact. Finally, the accuracy of the layered earth Green's functions for complex layer resistivities is tested using a three-layer model which has the properties and depth extent of the conductive prism of Figure A-3 but extends laterally to infinity. The dipole-dipole pseudosection for this layering was calculated using program EMIE3D (TFQ = 3) and compared to an analogous layered response computed using IP2DI. Agreement appears excellent.

Central loop magnetic field responses are demonstrated using the model of Figure A-4, which is a conductive (10 ohm-m) layer 200 m thick constructed as an inhomogeneity out of rectangular cells and residing in a 100 ohm-m half-space. The inhomogeneity has two symmetry planes with 124 cells per quadrant. Cells double in horizontal dimension outward from the center of the loop to the edge of the 3-D body at  $x$  and  $y = \pm 4250$  m, and thicken with distance also to economize on cell number. Magnetic fields are calculated at the center of the loop and compared to primary fields computed for a three-layer earth, with layer two being 10 ohm-m and the same as the prior 'layer' inhomogeneity, using program EMIE3D (TFQ = 3). The 3-D calculations on the 486/66 required 565 s to form the matrices, 340 s to solve them, and less than 5 s to compute the receiver fields. Results from multiple frequencies have been concatenated with a program

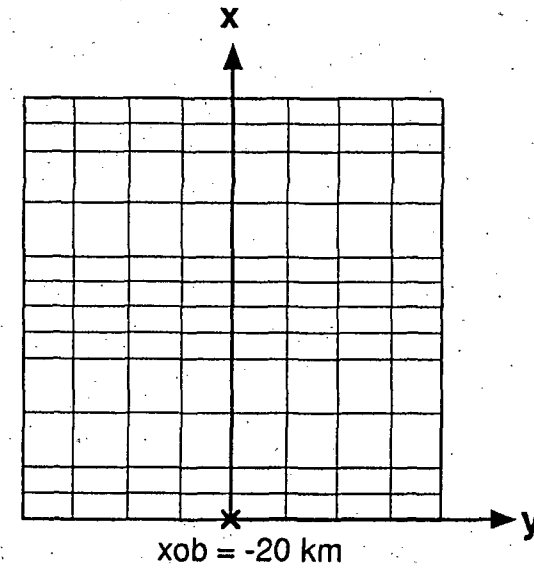
editor in the sample output. Agreement between the 3-D and the 1-D H-fields appears to be within 1% relative to the primary field up to about 1000 Hz, and somewhat worse at higher frequencies where cell thicknesses have exceeded one skin depth in 10 ohm-m. However, at these frequencies, the 100 ohm-m material in the upper 100 m dominates the departure from the free-space field as can be seen by the similarity of the primary fields HZON for the one-layer and three-layer host cases at the highest frequencies. The frequency of peak influence of the 10 ohm-m medium is about 500 Hz.

Small offset loop EM results are exemplified by simulating the same small 1 ohm-m prism in a half-space considered by Hohmann (1975) (Figure A-5). This body of two-fold symmetry has 24 cells per quadrant, the same as that of Hohmann, and is considered with a half-space host of 100 ohm-m. The accuracy of EMIE3D was verified by reproducing the responses computed and drawn by Hohmann (1975). Here, however, airborne results are computed 30 m above the surface for both HCP and VCA configurations for a source-receiver separation of 10 m and a frequency of 1000 Hz. The 3-D calculations on the 486/66 required 55 s to form the matrices, 30 s to solve them, and less than 5 s to compute the receiver fields. The airborne anomaly is fairly subdued as expected and peaks at a few tens of ppm in both real and imaginary components.

### Section View



### Plan View



A-1. Buried conductive (1 ohm-m) and resistive (100 ohm-m) elongate prisms in a three layer host. The structure has one vertical symmetry plane ( $x$ - $z$ ) on each side of which there are 80 cells.

0,1,3,1  
0.01  
10000.,30000.  
10.,100.,0.1  
8,1,1000.,1  
-25000.,0.,-16250.,0.,-10000.,0., -3750.,0.  
3750.,0., 10000.,0., 16250.,0., 25000.,0.  
0.0  
2,2,1,-20000.,0.  
1.,100.  
2500.,3750.,12,4  
2500.,2500.,5000.,5000.,2500.,2500.  
2500.,2500.,5000.,5000.,2500.,2500.  
5000.,5000.,5000.,5000.  
11111222222  
11111222222  
11111222222  
11111222222  
5000.,7500.,8,4  
5000.,5000.,5000.,5000.,5000.,5000.,5000.,5000.  
5000.,5000.,5000.,5000.  
11112222  
11112222  
11112222  
11112222



MAGNETOTELLURIC CALCULATIONS; NSTYP = 0

NFREQ = 1 NLYR = 3 NREC = 8

FREQ(I): 0.1000E-01

DEPL(I): 10000.00 30000.00

RHOL(I): 10.00 100.00 0.10

POLARIZATION 1 IS +X, POLARIZATION 2 IS +Y

ISYM = 1 NCEL = 80 NRES = 2

SITE LOCATION	X = -25000.0	Y = 0.0	Z = 0.0	FREQ = 0.1000E-01
EX01-EX02-EY01-EY02	0.4618E-05 0.3615E-05	0.0000E+00 0.0000E+00	0.0000E+00 0.0000E+00	0.4618E-05 0.3615E-05
HX01-HX02-HY01-HY02	0.0000E+00 0.0000E+00	-0.5309E-02 0.9178E-08	0.5309E-02-0.9178E-08	0.0000E+00 0.0000E+00
EXS1-EXS2-EYS1-EYS2	0.2841E-06-0.5283E-07	-0.2279E-12 0.1930E-12	0.9981E-13 0.1073E-12	-0.1879E-05-0.3725E-06
HXS1-HXS2-HYS1-HYS2	-0.5146E-11 0.1003E-12	0.1497E-03 0.1363E-03	0.1275E-03-0.2724E-04	-0.1157E-10-0.6522E-11
EZS1-EZS2-HZS1-HZS2	0.2239E-08 0.7177E-09	-0.4922E-13 0.1691E-13	0.3632E-12-0.3016E-12	0.1169E-02-0.2726E-03
EXT1-EXT2-EYT1-EYT2	0.4902E-05 0.3562E-05	0.5637E-11 0.1930E-12	0.5964E-11 0.1073E-12	0.2739E-05 0.3242E-05
HXT1-HXT2-HYT1-HYT2	0.5303E-08 0.1003E-12	-0.5159E-02 0.1363E-03	0.5436E-02-0.2725E-04	0.5297E-08-0.6522E-11
HZ01-HZ02-HZT1-HZT2	0.0000E+00 0.0000E+00	0.0000E+00 0.0000E+00	0.3632E-12-0.3016E-12	0.1169E-02-0.2726E-03
RXY1D-PXY1D-RYX1D-PYX1D	0.1546E+02 38.1	0.1546E+02 38.1		
RXYIN-PXYIN-RYXIN-PYXIN	0.1574E+02 36.3	0.8567E+01 51.3		
RXXIN-PXXIN-RYYIN-PYYIN	0.5529E-11 26.2	0.3765E-10 13.6		
RXYSC-PXYSC-RYXSC-PYXSC	0.1574E+02 36.3	0.8567E+01 51.3		
KZXIN-KZYIN-TIPH	-0.2278E+00 0.4682E-01	0.2226E-06-0.4462E-07	0.2326E+00	
MZ-STRIKE = 90.0	PZ-STRIKE = 90.0	KZ-STRIKE = 90.0		
SKEW-ELIP-SKWM-ELPM	0.9940E-06-0.4155E-08	-0.4662E-05 0.1604E-06	0.9940E-06 0.4664E-05	
RXYMZ-PXYMZ-RYXMZ-PYXMZ	0.8567E+01 51.3	0.1574E+02 36.3		
RXYKZ-PXYKZ-RYXKZ-PYXKZ	0.8567E+01 51.3	0.1574E+02 36.3		

SITE LOCATION	X = -16250.0	Y = 0.0	Z = 0.0	FREQ = 0.1000E-01
EX01-EX02-EY01-EY02	0.4618E-05 0.3615E-05	0.0000E+00 0.0000E+00	0.0000E+00 0.0000E+00	0.4618E-05 0.3615E-05
HX01-HX02-HY01-HY02	0.0000E+00 0.0000E+00	-0.5309E-02 0.9178E-08	0.5309E-02-0.9178E-08	0.0000E+00 0.0000E+00
EXS1-EXS2-EYS1-EYS2	-0.3121E-05-0.1355E-05	0.8131E-12-0.4860E-12	0.1168E-12 0.1611E-13	-0.2555E-05-0.1108E-05
HXS1-HXS2-HYS1-HYS2	0.6055E-11 0.3620E-11	-0.1337E-02 0.2217E-03	0.1486E-03-0.3562E-04	-0.1314E-10-0.1871E-12
EZS1-EZS2-HZS1-HZS2	0.4103E-08 0.8751E-09	-0.1791E-13-0.9939E-14	0.1171E-10 0.6833E-11	0.9133E-03-0.2564E-03
EXT1-EXT2-EYT1-EYT2	0.1497E-05 0.2260E-05	0.6678E-11-0.4860E-12	0.5981E-11 0.1611E-13	0.2063E-05 0.2507E-05
HXT1-HXT2-HYT1-HYT2	0.5315E-08 0.3620E-11	-0.6646E-02 0.2217E-03	0.5457E-02-0.3563E-04	0.5295E-08-0.1871E-12
HZ01-HZ02-HZT1-HZT2	0.0000E+00 0.0000E+00	0.0000E+00 0.0000E+00	0.1171E-10 0.6833E-11	0.9133E-03-0.2564E-03
RXY1D-PXY1D-RYX1D-PYX1D	0.1546E+02 38.1	0.1546E+02 38.1		
RXYIN-PXYIN-RYXIN-PYXIN	0.3125E+01 56.8	0.3019E+01 52.5		
RXXIN-PXXIN-RYYIN-PYYIN	0.9932E-11 11.2	0.2614E-10 8.9		
RXYSC-PXYSC-RYXSC-PYXSC	0.3125E+01 56.8	0.3019E+01 52.5		
KZXIN-KZYIN-TIPH	-0.1386E+00 0.3395E-01	0.1373E-06-0.3083E-07	0.1427E+00	
MZ-STRIKE = 90.0	PZ-STRIKE = 90.0	KZ-STRIKE = 90.0		
SKEW-ELIP-SKWM-ELPM	0.9777E-06-0.3185E-07	0.3751E-04 0.4215E-04	0.9782E-06 0.5643E-04	
RXYMZ-PXYMZ-RYXMZ-PYXMZ	0.3019E+01 52.5	0.3125E+01 56.8		
RXYKZ-PXYKZ-RYXKZ-PYXKZ	0.3019E+01 52.5	0.3125E+01 56.8		

SITE LOCATION	X =	Y =	Z =	FREQ =
EX01-EX02-EY01-EY02	-10000.0	0.0	0.0	0.1000E-01
HX01-HX02-HY01-HY02	0.4618E-05 0.3615E-05	0.0000E+00 0.0000E+00	0.0000E+00 0.0000E+00	0.4618E-05 0.3615E-05
EXS1-EXS2-EYS1-EYS2	0.0000E+00 0.0000E+00	-0.5309E-02 0.9178E-08	0.5309E-02-0.9178E-08	0.0000E+00 0.0000E+00
HXS1-HXS2-HYS1-HYS2	-0.3414E-05-0.1436E-05	-0.3862E-12-0.7921E-13	-0.1631E-12-0.9965E-13	-0.2683E-05-0.1270E-05
EZS1-EZS2-HZS1-HZS2	0.3725E-11 0.3274E-11	-0.1531E-02 0.3461E-03	0.6343E-04-0.3736E-04	0.3842E-11 0.1368E-11
EXT1-EXT2-EYT1-EYT2	0.8033E-10 0.2840E-09	-0.5237E-13-0.3155E-13	0.2934E-11 0.5034E-11	-0.1369E-03 0.1727E-05
HXT1-HXT2-HYT1-HYT2	0.1204E-05 0.2179E-05	0.5478E-11-0.7921E-13	0.5702E-11-0.9965E-13	0.1935E-05 0.2345E-05
HZ01-HZ02-HZT1-HZT2	0.5312E-08 0.3274E-11	-0.6840E-02 0.3461E-03	0.5372E-02-0.3737E-04	0.5312E-08 0.1368E-11
RXY1D-PXY1D-RYX1D-PYX1D	0.0000E+00 0.0000E+00	0.0000E+00 0.0000E+00	0.2934E-11 0.5034E-11	-0.1369E-03 0.1727E-05
RXYIN-PXYIN-RYXIN-PYXIN	0.1546E+02 38.1	0.1546E+02 38.1		
RXXIN-PXXIN-RYYIN-PYYIN	0.2721E+01 61.5	0.2496E+01 53.4		
RXYSC-PXYSC-RYXSC-PYXSC	0.6358E-11 9.6	0.2358E-10 8.1		
KZXIN-KZYIN-TIPH	0.2721E+01 61.5	0.2496E+01 53.4		
MZ-STRIKE = 90.0	0.1997E-01 0.7581E-03	-0.1920E-07 0.4168E-10	0.1999E-01	
SKEW-ELIP-SKWM-ELPM	PZ-STRIKE = 90.0	KZ-STRIKE = 90.0		
RXYMZ-PXYMZ-RYXMZ-PYXMZ	0.9965E-06-0.2516E-06	0.1845E-04 0.2275E-04	0.1028E-05 0.2929E-04	
RXYKZ-PXYKZ-RYXKZ-PYXKZ	0.2496E+01 53.4	0.2721E+01 61.5		

SITE LOCATION	X =	Y =	Z =	FREQ =
EX01-EX02-EY01-EY02	-3750.0	0.0	0.0	0.1000E-01
HX01-HX02-HY01-HY02	0.4618E-05 0.3615E-05	0.0000E+00 0.0000E+00	0.0000E+00 0.0000E+00	0.4618E-05 0.3615E-05
EXS1-EXS2-EYS1-EYS2	0.0000E+00 0.0000E+00	-0.5309E-02 0.9178E-08	0.5309E-02-0.9178E-08	0.0000E+00 0.0000E+00
HXS1-HXS2-HYS1-HYS2	-0.2708E-05-0.1105E-05	-0.1488E-11 0.2401E-12	-0.1802E-12-0.1196E-13	-0.2569E-05-0.9466E-06
EZS1-EZS2-HZS1-HZS2	-0.5289E-11-0.3148E-11	-0.1272E-02 0.7892E-04	-0.1211E-03-0.2917E-04	-0.6541E-11-0.8324E-11
EXT1-EXT2-EYT1-EYT2	-0.7006E-08-0.2948E-08	-0.7497E-13-0.3311E-13	0.2085E-11-0.6126E-12	-0.1244E-02 0.1327E-03
HXT1-HXT2-HYT1-HYT2	0.1910E-05 0.2510E-05	0.4377E-11 0.2401E-12	0.5684E-11-0.1196E-13	0.2049E-05 0.2668E-05
HZ01-HZ02-HZT1-HZT2	0.5303E-08-0.3148E-11	-0.6580E-02 0.7893E-04	0.5188E-02-0.2918E-04	0.5302E-08-0.8324E-11
RXY1D-PXY1D-RYX1D-PYX1D	0.0000E+00 0.0000E+00	0.0000E+00 0.0000E+00	0.2085E-11-0.6126E-12	-0.1244E-02 0.1327E-03
RXYIN-PXYIN-RYXIN-PYXIN	0.1546E+02 38.1	0.1546E+02 38.1		
RXXIN-PXXIN-RYYIN-PYYIN	0.4682E+01 53.1	0.3310E+01 53.2		
RXYSC-PXYSC-RYXSC-PYXSC	0.3327E-11 13.3	0.2734E-10 9.6		
KZXIN-KZYIN-TIPH	0.4682E+01 53.1	0.3310E+01 53.2		
MZ-STRIKE = 90.0	0.1893E+00-0.1790E-01	-0.1932E-06 0.1720E-07	0.1901E+00	
SKEW-ELIP-SKWM-ELPM	PZ-STRIKE = 90.0	KZ-STRIKE = 90.0		
RXYMZ-PXYMZ-RYXMZ-PYXMZ	0.1107E-05-0.3228E-06	-0.1184E-04 0.1413E-04	0.1153E-05 0.1844E-04	
RXYKZ-PXYKZ-RYXKZ-PYXKZ	0.3310E+01 53.2	0.4682E+01 53.1		

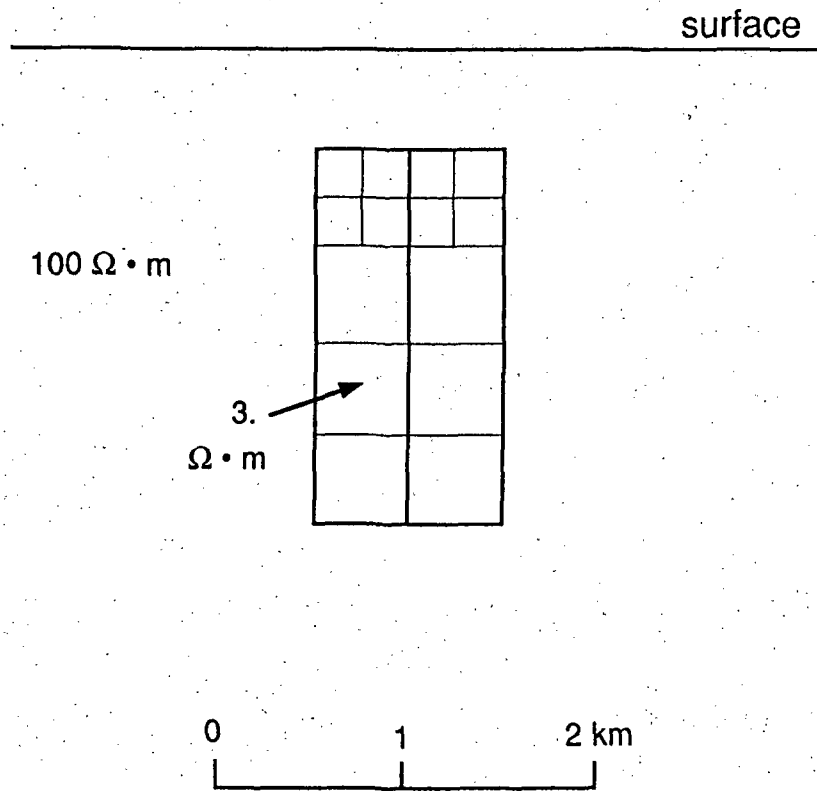
SITE LOCATION	X =	Y =	Z =	FREQ =
EX01-EX02-EY01-EY02	3750.0	0.0	0.0	0.1000E-01
HX01-HX02-HY01-HY02	0.4618E-05 0.3615E-05	0.0000E+00 0.0000E+00	0.0000E+00 0.0000E+00	0.4618E-05 0.3615E-05
EXS1-EXS2-EYS1-EYS2	0.0000E+00 0.0000E+00	-0.5309E-02 0.9178E-08	0.5309E-02-0.9178E-08	0.0000E+00 0.0000E+00
HXS1-HXS2-HYS1-HYS2	0.3491E-05 0.2188E-05	0.1336E-11 0.2464E-13	-0.2579E-12-0.2327E-13	-0.1815E-05 0.4068E-08
EZS1-EZS2-HZS1-HZS2	0.1051E-11-0.3994E-11	0.3805E-03 0.2357E-03	-0.3679E-03-0.5681E-04	-0.2545E-11 0.5290E-12
EXT1-EXT2-EYT1-EYT2	-0.3855E-08-0.2321E-08	-0.1881E-13-0.9816E-14	-0.1088E-10-0.6611E-11	-0.1551E-02-0.8263E-05
HXT1-HXT2-HYT1-HYT2	0.8109E-05 0.5803E-05	0.7201E-11 0.2464E-13	0.5607E-11-0.2327E-13	0.2803E-05 0.3619E-05
HZ01-HZ02-HZT1-HZT2	0.5310E-08-0.3994E-11	-0.4928E-02 0.2357E-03	0.4941E-02-0.5682E-04	0.5306E-08 0.5290E-12
RXY1D-PXY1D-RYX1D-PYX1D	0.0000E+00 0.0000E+00	0.0000E+00 0.0000E+00	-0.1088E-10-0.6611E-11	-0.1551E-02-0.8263E-05
RXYIN-PXYIN-RYXIN-PYXIN	0.1546E+02 38.1	0.1546E+02 38.1		
RXXIN-PXXIN-RYYIN-PYYIN	0.5159E+02 36.2	0.1090E+02 55.0		
RXYSC-PXYSC-RYXSC-PYXSC	0.2178E-10 44.1	0.4527E-10 16.5		
KZXIN-KZYIN-TIPH	0.5159E+02 36.2	0.1090E+02 55.0		
MZ-STRIKE = 90.0	0.3139E+00 0.1669E-01	-0.3392E-06-0.2292E-07	0.3143E+00	
SKEW-ELIP-SKWM-ELPM	PZ-STRIKE = 90.0	KZ-STRIKE = 90.0		
RXYMZ-PXYMZ-RYXMZ-PYXMZ	0.9796E-06 0.9656E-07	-0.1052E-05 0.8221E-06	0.9844E-06 0.1335E-05	
RXYKZ-PXYKZ-RYXKZ-PYXKZ	0.1090E+02 55.0	0.5159E+02 36.2		

SITE LOCATION	X = 10000.0	Y = 0.0	Z = 0.0	FREQ = 0.1000E-01
EX01-EX02-EY01-EY02	0.4618E-05	0.3615E-05	0.0000E+00	0.0000E+00
HX01-HX02-HY01-HY02	0.0000E+00	0.0000E+00	-0.5309E-02	0.9178E-08
EXS1-EXS2-EYS1-EYS2	0.3274E-05	0.2120E-05	0.3892E-12	-0.1012E-13
HXS1-HXS2-HYS1-HYS2	0.6580E-12	-0.1398E-11	0.8317E-03	0.2340E-03
EZS1-EZS2-HZS1-HZS2	0.1099E-08	-0.3359E-09	0.9301E-13	-0.4726E-14
EXT1-EXT2-EYT1-EYT2	0.7892E-05	0.5735E-05	0.6254E-11	-0.1012E-13
HXT1-HXT2-HYT1-HYT2	0.5309E-08	-0.1398E-11	-0.4477E-02	0.2340E-03
HZ01-HZ02-HZT1-HZT2	0.0000E+00	0.0000E+00	0.0000E+00	0.0000E+00
RXY1D-PXY1D-RYX1D-PYX1D	0.1546E+02	38.1	0.1546E+02	38.1
RXYIN-PXYIN-RYXIN-PYXIN	0.5037E+02	36.7	0.1887E+02	52.1
RXXIN-PXXIN-RYYIN-PYYIN	0.2832E-10	43.1	0.6450E-10	18.9
RXYSC-PXYSC-RYXSC-PYXSC	0.5037E+02	36.7	0.1887E+02	52.1
KZXIN-KZYIN-TIPH	0.1696E+00	-0.2856E-01	-0.1848E-06	0.2811E-07
MZ-STRIKE = 90.0	PZ-STRIKE = 90.0	KZ-STRIKE = 90.0		0.1720E+00
SKEW-ELIP-SKWM-ELPM	0.1088E-05	0.6427E-07	-0.1646E-05	0.8687E-06
RXYMZ-PXYMZ-RYXMZ-PYXMZ	0.1887E+02	52.1	0.5037E+02	36.7
RXYKZ-PXYKZ-RYXKZ-PYXKZ	0.1887E+02	52.1	0.5037E+02	36.7

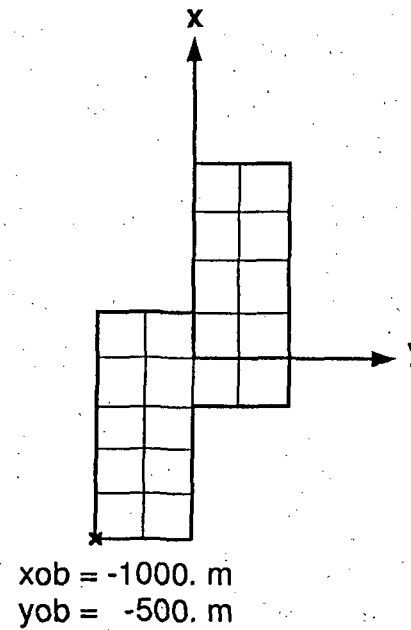
SITE LOCATION	X = 16250.0	Y = 0.0	Z = 0.0	FREQ = 0.1000E-01
EX01-EX02-EY01-EY02	0.4618E-05	0.3615E-05	0.0000E+00	0.0000E+00
HX01-HX02-HY01-HY02	0.0000E+00	0.0000E+00	-0.5309E-02	0.9178E-08
EXS1-EXS2-EYS1-EYS2	0.3248E-05	0.2148E-05	0.1456E-12	-0.1336E-12
HXS1-HXS2-HYS1-HYS2	0.8949E-12	0.2269E-11	0.7729E-03	0.1429E-03
EZS1-EZS2-HZS1-HZS2	0.3790E-08	0.1518E-08	0.9491E-13	-0.1382E-13
EXT1-EXT2-EYT1-EYT2	0.7866E-05	0.5763E-05	0.6010E-11	-0.1336E-12
HXT1-HXT2-HYT1-HYT2	0.5309E-08	0.2269E-11	-0.4536E-02	0.1429E-03
HZ01-HZ02-HZT1-HZT2	0.0000E+00	0.0000E+00	0.0000E+00	0.0000E+00
RXY1D-PXY1D-RYX1D-PYX1D	0.1546E+02	38.1	0.1546E+02	38.1
RXYIN-PXYIN-RYXIN-PYXIN	0.5048E+02	36.9	0.2155E+02	47.8
RXXIN-PXXIN-RYYIN-PYYIN	0.2945E-10	42.0	0.7465E-10	18.2
RXYSC-PXYSC-RYXSC-PYXSC	0.5048E+02	36.9	0.2155E+02	47.8
KZXIN-KZYIN-TIPH	0.2557E-01	-0.6491E-01	-0.2958E-07	0.6989E-07
MZ-STRIKE = 90.0	PZ-STRIKE = 90.0	KZ-STRIKE = 90.0		0.6977E-01
SKEW-ELIP-SKWM-ELPM	0.1117E-05	0.4254E-07	-0.2002E-05	0.1131E-05
RXYMZ-PXYMZ-RYXMZ-PYXMZ	0.2155E+02	47.8	0.5048E+02	36.9
RXYKZ-PXYKZ-RYXKZ-PYXKZ	0.2155E+02	47.8	0.5048E+02	36.9

SITE LOCATION	X = 25000.0	Y = 0.0	Z = 0.0	FREQ = 0.1000E-01
EX01-EX02-EY01-EY02	0.4618E-05	0.3615E-05	0.0000E+00	0.0000E+00
HX01-HX02-HY01-HY02	0.0000E+00	0.0000E+00	-0.5309E-02	0.9178E-08
EXS1-EXS2-EYS1-EYS2	-0.5687E-06	0.6536E-07	-0.2287E-12	0.4500E-13
HXS1-HXS2-HYS1-HYS2	0.1856E-12	-0.5673E-12	0.2444E-03	-0.1088E-03
EZS1-EZS2-HZS1-HZS2	0.2739E-08	0.1795E-08	0.4941E-13	-0.1185E-13
EXT1-EXT2-EYT1-EYT2	0.4049E-05	0.3680E-05	0.5636E-11	0.4500E-13
HXT1-HXT2-HYT1-HYT2	0.5309E-08	-0.5673E-12	-0.5064E-02	-0.1088E-03
HZ01-HZ02-HZT1-HZT2	0.0000E+00	0.0000E+00	0.0000E+00	0.0000E+00
RXY1D-PXY1D-RYX1D-PYX1D	0.1546E+02	38.1	0.1546E+02	38.1
RXYIN-PXYIN-RYXIN-PYXIN	0.1520E+02	42.4	0.1813E+02	40.7
RXXIN-PXXIN-RYYIN-PYYIN	0.8271E-11	29.6	0.6889E-10	14.7
RXYSC-PXYSC-RYXSC-PYXSC	0.1520E+02	42.4	0.1813E+02	40.7
KZXIN-KZYIN-TIPH	-0.4163E-01	-0.4911E-01	0.4401E-07	0.5217E-07
MZ-STRIKE = 90.0	PZ-STRIKE = 90.0	KZ-STRIKE = 90.0		0.6439E-01
SKEW-ELIP-SKWM-ELPM	0.1098E-05	-0.2331E-07	0.2361E-04	-0.7765E-05
RXYMZ-PXYMZ-RYXMZ-PYXMZ	0.1813E+02	40.7	0.1520E+02	42.4
RXYKZ-PXYKZ-RYXKZ-PYXKZ	0.1813E+02	40.7	0.1520E+02	42.4

## Section View



## Plan View



A-2. Offset conductive (3 ohm-m) prism model in a resistive (100 ohm-m) host used to demonstrate tensor CSAMT calculations for a body with no planes of symmetry. There are 58 cells in this body and grounded bipole sources are placed at  $y = -30$  km. Results are compared to those for purely plane-wave excitation.

1,1,1,1  
30.  
100.  
5,1,250.,1,1  
0., 0., 0., 750., 500., 250., 1250., 0., 750.,1250.  
0.0  
15000.,-30000.,15000.,-30000.  
1000.,0.,1000.,90.  
1,5,0,-1000.,-500.  
3.  
250.,375.,8,4  
250.,250.,250.,250.,250.,250.,250.,250.  
250.,250.,250.,250.  
11111000  
11111000  
00011111  
00011111  
250.,625.,8,4  
250.,250.,250.,250.,250.,250.,250.,250.  
250.,250.,250.,250.  
11111000  
11111000  
00011111  
00011111  
500.,1000.,5,2  
250.,500.,500.,500.,250.  
500.,500.  
11100  
00111  
500.,1500.,5,2  
250.,500.,500.,500.,250.  
500.,500.  
11100  
00111  
500.,2000.,5,2  
250.,500.,500.,500.,250.  
500.,500.  
11100  
00111

CSAMT TENSOR QUANTITIES, NSTYP = 1

NFREQ = 1 NLYR = 1 NREC = 5 KGRND = 1

FREQ(I): 0.3000E+02

RHOL(I): 100.00

SOURCE 1 AT X = 15000. Y = -30000.

LENGTH IS 1000. M, AZIMUTH IS 15.

SOURCE 2 AT X = 15000. Y = -30000.

LENGTH IS 1000. M, AZIMUTH IS 130.

RECEIVER POSITIONS (X,Y)

0.00	0.00	0.00	750.00	500.00	250.00	1250.00	0.00
750.00	1250.00						

ISYM = 0 NCEL = 58 NRES = 1

SITE LOCATION	X =	0.0	Y =	0.0	Z =	0.0	FREQ =	0.3000E+02
EX01-EX02-EY01-EY02	-0.6996E-09	-0.9457E-14	-0.9376E-11	0.1475E-13	-0.4447E-09	0.2040E-14	0.4564E-09	-0.2551E-13
HX01-HX02-HY01-HY02	0.2042E-08	-0.2038E-08	-0.2089E-08	0.2086E-08	-0.3217E-08	0.3210E-08	-0.3844E-10	0.3924E-10
EXS1-EXS2-EYS1-EYS2	0.2196E-09	-0.1226E-09	0.1094E-10	-0.5378E-11	0.1001E-09	-0.3485E-10	-0.1440E-09	0.7150E-10
HXS1-HXS2-HYS1-HYS2	0.2126E-09	-0.5676E-09	-0.1071E-09	0.2646E-09	-0.1770E-09	0.6994E-09	0.3211E-10	-0.8104E-10
EZS1-EZS2-HZS1-HZS2	-0.5690E-14	-0.4111E-14	0.1442E-13	0.1061E-13	-0.4134E-12	-0.2529E-11	-0.3102E-11	0.9608E-11
EXT1-EXT2-EYT1-EYT2	-0.4800E-09	-0.1226E-09	0.1566E-11	-0.5364E-11	-0.3446E-09	-0.3485E-10	0.3124E-09	0.7147E-10
HXT1-HXT2-HYT1-HYT2	0.2255E-08	-0.2606E-08	-0.2196E-08	0.2351E-08	-0.3394E-08	0.3909E-08	-0.6327E-11	-0.4180E-10
HZ01-HZ02-HZT1-HZT2	0.1504E-12	-0.1537E-09	-0.3600E-13	0.3650E-10	-0.2630E-12	-0.1562E-09	-0.3138E-11	0.4610E-10
RXY1D-PXY1D-RYX1D-PYX1D	0.1003E+03	44.9	0.1009E+03	45.0				
RXY1N-PXY1N-RYX1N-PYX1N	0.3910E+02	63.7	0.4194E+02	59.9				
RXX1N-PXX1N-RYY1N-PYY1N	0.5029E-02	73.3	0.1416E+00	27.3				
RXYSC-PXYSC-RYXSC-PYXSC	0.3867E+02	63.4	0.4189E+02	59.8				
KZX1N-KZY1N-TIPH	0.1116E-01	-0.8798E-02	-0.1534E-01	0.1395E-01	0.2513E-01			
MZ-STRIKE = 184.0	PZ-STRIKE = 248.0		KZ-STRIKE = 214.0					
SKEW-ELIP-SKWM-ELPM	0.4458E-02	-0.2563E-01	0.9425E+00	-0.6311E+00	0.2602E-01	0.1134E+01		
RXYMZ-PXYMZ-RYXMZ-PYXMZ	0.3906E+02	63.4	0.4195E+02	60.1				
RXYKZ-PXYKZ-RYXKZ-PYXKZ	0.3969E+02	60.7	0.4127E+02	62.8				

SITE LOCATION	X =	0.0	Y =	750.0	Z =	0.0	FREQ =	0.3000E+02
EX01-EX02-EY01-EY02	-0.6664E-09	0.9744E-14	0.2695E-11	0.1457E-14	-0.4098E-09	0.6770E-14	0.4324E-09	-0.9582E-14
HX01-HX02-HY01-HY02	0.1881E-08	-0.1877E-08	-0.1972E-08	0.1970E-08	-0.3065E-08	0.3059E-08	0.2008E-10	-0.1921E-10
EXS1-EXS2-EYS1-EYS2	0.1228E-09	-0.1056E-09	-0.1177E-10	0.1392E-10	0.2811E-10	-0.3809E-11	0.2028E-11	-0.1761E-10
HXS1-HXS2-HYS1-HYS2	-0.3137E-10	-0.1242E-09	-0.2187E-10	0.1159E-09	0.1320E-09	-0.2480E-11	-0.1959E-10	0.7917E-11
EZS1-EZS2-HZS1-HZS2	0.8013E-13	0.5253E-13	-0.1114E-12	-0.1244E-12	-0.1355E-09	0.5660E-09	0.9582E-11	-0.5976E-10
EXT1-EXT2-EYT1-EYT2	-0.5436E-09	-0.1056E-09	-0.9076E-11	0.1392E-10	-0.3817E-09	-0.3802E-11	0.4344E-09	-0.1762E-10
HXT1-HXT2-HYT1-HYT2	0.1849E-08	-0.2001E-08	-0.1994E-08	0.2086E-08	-0.2933E-08	0.3056E-08	0.4898E-12	-0.1129E-10
HZ01-HZ02-HZT1-HZT2	-0.1615E-12	-0.1425E-09	0.3923E-13	0.3514E-10	-0.1356E-09	0.4236E-09	0.9621E-11	-0.2462E-10
RXY1D-PXY1D-RYX1D-PYX1D	0.1004E+03	44.9	0.1016E+03	45.0				
RXY1N-PXY1N-RYX1N-PYX1N	0.7395E+02	55.6	0.9581E+02	44.0				
RXX1N-PXX1N-RYY1N-PYY1N	0.1640E+00	8.6	0.3639E+00	1.8				

RXYSC-PXYSC-RYXSC-PYXSC	0.7215E+02	57.2	0.9581E+02	44.0
KZXIN-KZYIN-TIPH	-0.8321E-02	0.3125E-02	0.8900E-01-0.4402E-01	0.9969E-01
MZ-STRIKE = 193.0	PZ-STRIKE = 12.0		KZ-STRIKE = 185.0	
SKEW-ELIP-SKWM-ELPM	-0.1050E-01	0.5581E-02	0.2765E-01-0.3579E-01	0.1189E-01 0.4523E-01
RXYMZ-PXYMZ-RYXMZ-PYXMZ	0.7282E+02	56.2	0.9745E+02	43.5
RXYKZ-PXYKZ-RYXKZ-PYXKZ	0.7329E+02	56.0	0.9679E+02	43.7

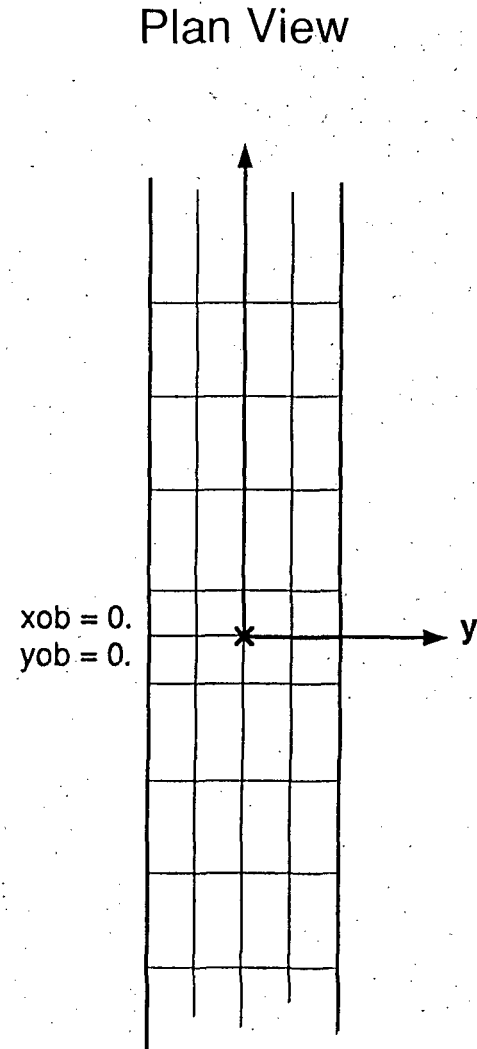
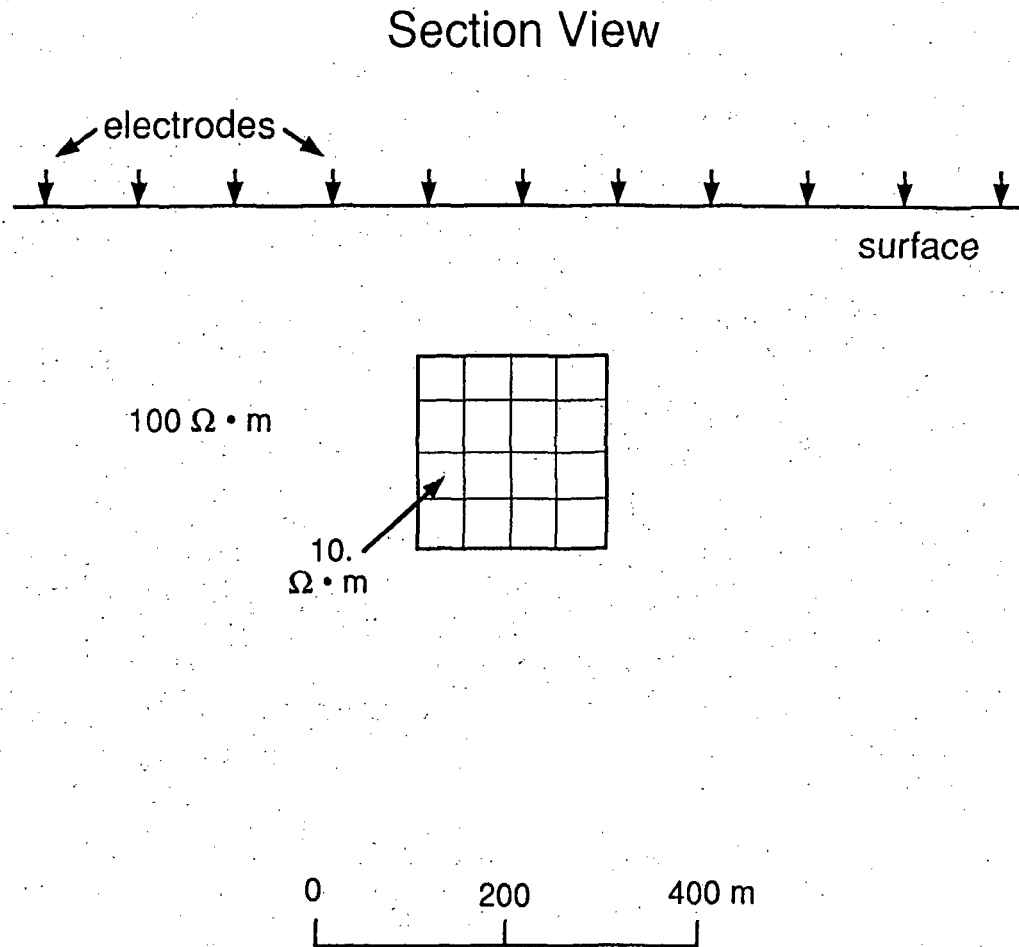
SITE LOCATION	X =	500.0	Y =	250.0	Z =	0.0	FREQ =	0.3000E+02
EX01-EX02-EY01-EY02	-0.7120E-09-0.9100E-14		0.1119E-10 0.1430E-13		-0.4276E-09 0.1775E-14		0.4607E-09-0.2548E-13	
HX01-HX02-HY01-HY02	0.1964E-08-0.1961E-08		-0.2109E-08 0.2106E-08		-0.3274E-08 0.3267E-08		0.5624E-10-0.5528E-10	
EXS1-EXS2-EYS1-EYS2	0.1927E-09-0.1018E-09		0.6867E-11-0.4028E-11		0.1082E-09-0.5739E-10		-0.1286E-09 0.7326E-10	
HXS1-HXS2-HYS1-HYS2	0.4312E-10-0.2385E-09		-0.2227E-10 0.1071E-09		-0.2547E-09 0.7473E-09		0.3452E-10-0.1078E-09	
EZS1-EZS2-HZS1-HZS2	0.4621E-12 0.1216E-12		-0.9544E-13-0.4252E-13		0.2858E-10-0.9570E-10		-0.4519E-10 0.1454E-09	
EXT1-EXT2-EYT1-EYT2	-0.5192E-09-0.1018E-09		0.1805E-10-0.4014E-11		-0.3195E-09-0.5739E-10		0.3320E-09 0.7324E-10	
HXT1-HXT2-HYT1-HYT2	0.2008E-08-0.2199E-08		-0.2131E-08 0.2213E-08		-0.3529E-08 0.4014E-08		0.9076E-10-0.1631E-09	
HZ01-HZ02-HZT1-HZT2	0.1487E-12-0.1541E-09		-0.3796E-13 0.3901E-10		0.2873E-10-0.2498E-09		-0.4522E-10 0.1845E-09	
RXY1D-PXY1D-RYX1D-PYX1D	0.1003E+03	44.9	0.1009E+03	45.0				
RXYIN-PXYIN-RYXIN-PYXIN	0.4157E+02	60.1	0.5178E+02	58.5				
RXXIN-PXXIN-RYYIN-PYYIN	0.6451E-02	51.0	0.6663E-02	81.4				
RXYSC-PXYSC-RYXSC-PYXSC	0.4138E+02	59.8	0.5171E+02	58.5				
KZXIN-KZYIN-TIPH	0.5311E-01-0.3029E-01		-0.8752E-02 0.1050E-01		0.6265E-01			
MZ-STRIKE = 93.0	PZ-STRIKE = 254.0		KZ-STRIKE = 258.0					
SKEW-ELIP-SKWM-ELPM	-0.2589E-02 0.1731E-02		0.2772E-01-0.1878E+00		0.3114E-02 0.1898E+00			
RXYMZ-PXYMZ-RYXMZ-PYXMZ	0.5182E+02	58.6	0.4154E+02	60.1				
RXYKZ-PXYKZ-RYXKZ-PYXKZ	0.5105E+02	58.4	0.4224E+02	60.3				

SITE LOCATION	X =	1250.0	Y =	0.0	Z =	0.0	FREQ =	0.3000E+02
EX01-EX02-EY01-EY02	-0.7609E-09-0.2380E-13		0.3427E-10 0.2427E-13		-0.4305E-09-0.2337E-14		0.4878E-09-0.3837E-13	
HX01-HX02-HY01-HY02	0.1979E-08-0.1975E-08		-0.2240E-08 0.2237E-08		-0.3499E-08 0.3491E-08		0.1596E-09-0.1584E-09	
EXS1-EXS2-EYS1-EYS2	0.7541E-11 0.3824E-10		-0.1685E-10 0.8877E-11		0.6998E-10-0.7853E-10		-0.3765E-10 0.3318E-10	
HXS1-HXS2-HYS1-HYS2	-0.8571E-10 0.1364E-09		0.4175E-10-0.4796E-10		0.1309E-10 0.2408E-09		-0.2470E-10-0.3335E-11	
EZS1-EZS2-HZS1-HZS2	0.2573E-12 0.1353E-12		-0.1213E-13 0.1212E-13		0.5616E-10-0.2549E-09		-0.4084E-10 0.1393E-09	
EXT1-EXT2-EYT1-EYT2	-0.7534E-09 0.3822E-10		0.1742E-10 0.8901E-11		-0.3605E-09-0.7853E-10		0.4502E-09 0.3314E-10	
HXT1-HXT2-HYT1-HYT2	0.1893E-08-0.1838E-08		-0.2198E-08 0.2189E-08		-0.3486E-08 0.3732E-08		0.1349E-09-0.1617E-09	
HZ01-HZ02-HZT1-HZT2	0.4022E-12-0.1650E-09		-0.1084E-12 0.4444E-10		0.5656E-10-0.4199E-09		-0.4094E-10 0.1837E-09	
RXY1D-PXY1D-RYX1D-PYX1D	0.1002E+03	44.9	0.1003E+03	45.0				
RXYIN-PXYIN-RYXIN-PYXIN	0.9525E+02	43.3	0.8967E+02	48.8				
RXXIN-PXXIN-RYYIN-PYYIN	0.1565E+00	2.7	0.4447E+00	17.3				
RXYSC-PXYSC-RYXSC-PYXSC	0.9214E+02	44.0	0.8940E+02	49.1				
KZXIN-KZYIN-TIPH	0.4852E-01-0.3011E-01		-0.4185E-01 0.3372E-01		0.7842E-01			
MZ-STRIKE = 239.0	PZ-STRIKE = 68.0		KZ-STRIKE = 227.0					
SKEW-ELIP-SKWM-ELPM	-0.5886E-03 0.1690E-01		-0.2574E+00 0.1561E+00		0.1691E-01 0.3011E+00			
RXYMZ-PXYMZ-RYXMZ-PYXMZ	0.8640E+02	49.7	0.9897E+02	42.6				
RXYKZ-PXYKZ-RYXKZ-PYXKZ	0.8671E+02	48.9	0.9834E+02	43.3				

SITE LOCATION	X =	750.0	Y =	1250.0	Z =	0.0	FREQ =	0.3000E+02
EX01-EX02-EY01-EY02	-0.6766E-09 0.1384E-13		0.3289E-10-0.1656E-14		-0.3801E-09 0.7299E-14		0.4329E-09-0.6565E-14	
HX01-HX02-HY01-HY02	0.1745E-08-0.1741E-08		-0.1974E-08 0.1972E-08		-0.3112E-08 0.3105E-08		0.1588E-09-0.1577E-09	
EXS1-EXS2-EYS1-EYS2	0.3252E-10-0.3347E-10		0.4605E-11-0.7064E-11		-0.1601E-10 0.4463E-10		0.3658E-11-0.1342E-10	
HXS1-HXS2-HYS1-HYS2	0.1346E-11-0.1539E-09		0.3417E-11 0.4241E-10		0.7673E-10-0.6036E-10		0.8229E-11-0.3332E-10	
EZS1-EZS2-HZS1-HZS2	0.1007E-12 0.5089E-13		-0.4919E-13-0.3624E-13		0.1462E-10 0.2005E-09		-0.3140E-11 0.1686E-10	
EXT1-EXT2-EYT1-EYT2	-0.6441E-09-0.3345E-10		0.3750E-10-0.7066E-11		-0.3961E-09 0.4464E-10		0.4366E-09-0.1343E-10	
HXT1-HXT2-HYT1-HYT2	0.1746E-08-0.1895E-08		-0.1970E-08 0.2014E-08		-0.3035E-08 0.3045E-08		0.1671E-09-0.1911E-09	
HZ01-HZ02-HZT1-HZT2	-0.2232E-12-0.1410E-09		0.5978E-13 0.3822E-10		0.1440E-10 0.5953E-10		-0.3080E-11 0.5508E-10	
RXY1D-PXY1D-RYX1D-PYX1D	0.1004E+03	44.9	0.1017E+03	45.0				
RXYIN-PXYIN-RYXIN-PYXIN	0.9535E+02	48.6	0.1016E+03	44.0				
RXXIN-PXXIN-RYYIN-PYYIN	0.2573E-01	49.7	0.1075E+00	52.5				

RXWSC-PXWSC-RXWSC-PYWSC	0.9501E+02	48.1	0.1015E+03	43.9	
KZXIN-KZYIN-TIPH	0.1614E-01-0.1490E-01		0.1676E-01-0.2145E-01		0.3498E-01
MZ-STRIKE = 184.0	PZ-STRIKE = 165.0		KZ-STRIKE = 141.0		
SKEW-ELIP-SKWM-ELPM	-0.1686E-02-0.8296E-02		0.6723E+00-0.3301E+00		0.8465E-02 0.7490E+00
RXYMZ-PXYMZ-RYXMZ-PYXMZ	0.9526E+02	48.4	0.1016E+03	44.2	
RXYKZ-PXYKZ-RYXKZ-PYXKZ	0.9838E+02	48.1	0.9837E+02	44.4	





A-3. Buried conductive (10 ohm-m) elongate prism in a resistive half-space host (100 ohm-m). The body is polarizable with an intrinsic IP effect of 6 mrad. The structure has two symmetry planes with 64 cells per quadrant and is simulated for the dipole-dipole resistivity/IP array. Results are compared to those of the UURI 2-D finite element program, IP2DI-v1.00, and to coupling values in Millett's tables.

2,1,1,1  
.0001  
100.  
16,1,100.,90.,8,1  
0.,0.  
1,4,2,0.,0.  
10.  
6.  
50.,175.,8,2  
50.,100.,100.,200.,300.,400.,600.,750.  
50.,50.  
11111111  
11111111  
50.,225.,8,2  
50.,100.,100.,200.,300.,400.,600.,750.  
50.,50.  
11111111  
11111111  
50.,275.,8,2  
50.,100.,100.,200.,300.,400.,600.,750.  
50.,50.  
11111111  
11111111  
50.,325.,8,2  
50.,100.,100.,200.,300.,400.,600.,750.  
50.,50.  
11111111  
11111111



APPARENT IP EFFECT, FREQ = 0.1000E-03

-7 -6 -5 -4 -3 -2 -1 0 +1 +2 +3 +4 +5 +6 +7  
-----

0.0	0.0	0.0	0.0	0.0	0.0	0.0	0.0	0.0	0.0	0.0	0.0	0.0	0.0	0.0
0.0	0.0	-0.1	-0.1	0.0	0.2	0.3	0.2	0.0	-0.1	-0.1	0.0	0.0		
-0.1	-0.1	-0.1	0.1	0.4	0.6	0.6	0.4	0.1	-0.1	-0.1	-0.1			
-0.1	-0.1	0.1	0.5	0.9	1.0	0.9	0.5	0.1	-0.1	-0.1				
	-0.2	0.1	0.6	1.1	1.2	1.2	1.1	0.6	0.1	-0.2				
		0.1	0.7	1.2	1.2	1.2	1.3	1.2	0.7	0.1				
			0.8	1.2	1.2	1.2	1.2	1.2	1.2	0.8				
				1.2	1.2	1.2	1.2	1.2	1.2	1.2				







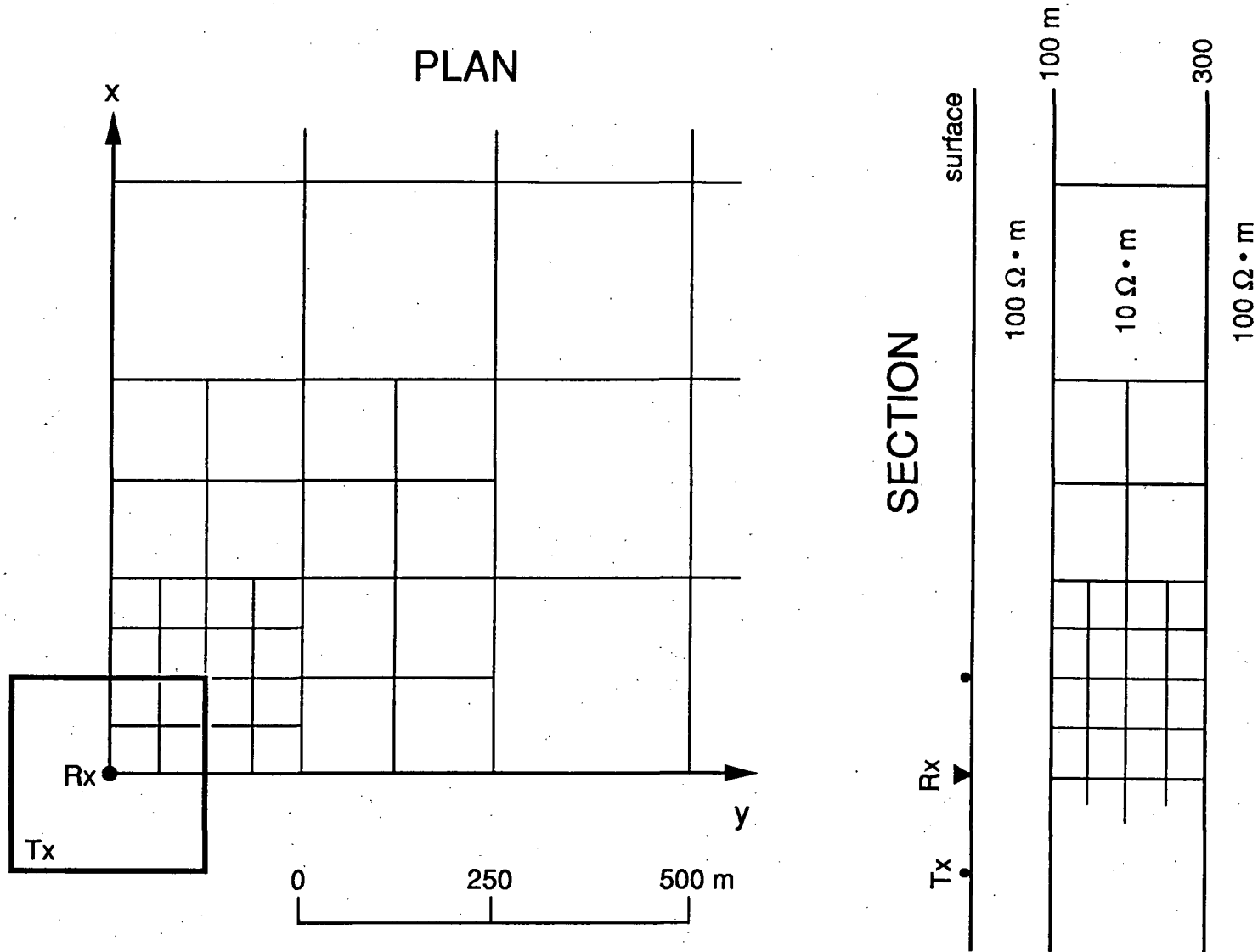


Figure A-4. Buried low-resistivity (10 ohm-m) layer constructed as an inhomogeneity in a 100 ohm-m half-space. The structure has two symmetry planes with 124 cells per quadrant and is simulated for the central loop configuration with a magnetic field receiver at the center. Cells double in horizontal dimension outward from the center of the loop to the edge of the 3-D body at  $x$  and  $y = \pm 4250$  m, and thicken with distance also to economize on cell number.



4,10,1,1  
2500.,2000.,1500.,1000.,500.,250.,100.,50.,25.,10.  
100.  
1,1,250.,90.,1  
0.,0.  
0.,0.  
1,9,2,0.,0.  
10.  
50.,125.,4,4  
62.5,62.5,62.5,62.5  
62.5,62.5,62.5,62.5  
1111  
1111  
1111  
1111  
50.,175.,4,4  
62.5,62.5,62.5,62.5  
62.5,62.5,62.5,62.5  
1111  
1111  
1111  
1111  
50.,225.,4,4  
62.5,62.5,62.5,62.5  
62.5,62.5,62.5,62.5  
1111  
1111  
1111  
1111  
50.,275.,4,4  
62.5,62.5,62.5,62.5  
62.5,62.5,62.5,62.5  
1111  
1111  
1111  
1111  
100.,150.,4,4  
125.,125.,125.,125.  
125.,125.,125.,125.  
0011  
0011  
1111  
1111  
100.,250.,4,4  
125.,125.,125.,125.  
125.,125.,125.,125.  
0011  
0011  
1111  
1111  
200.,200.,4,4  
250.,250.,250.,250.  
250.,250.,250.,250.  
0011  
0011  
1111  
1111  
200.,200.,4,4  
500.,500.,500.,500.  
500.,500.,500.,500.

0011

0011

1111

1111

200.,200.,4,4

1000.,1000.,1000.,1000.

1000.,1000.,1000.,1000.

0011

0011

1111

1111

CENTRAL LOOP H-FIELDS (NSTYP = 4), NORMALIZED BY H-FS

NFREQ = 10 NLYR = 1 NSRC = 1 NLPSEP = 1

FREQ(I): 0.2500E+04 0.2000E+04 0.1500E+04 0.1000E+04 0.5000E+03 0.2500E+03 0.1000E+03 0.5000E+02 0.2500E+02 0.1000

RHOL(I): 100.00

LOOP SIDE LENGTH IS 250.0 M, PROFILE AZIMUTH IS 90.

SOURCE CENTER POSITIONS ----- (X,Y,Z)

0.00 0.00

RECEIVER POSITIONS W.R.T. SOURCE CENTER

0.00 0.00

ISYM = 2 NCEL = 124 NRES = 1

FREQ	XSRC	YSRC	XREC	YREC	ZREC	HZSN (Re,Im)		HZON (Re,Im)		HZT (Re,Im)	
0.2500E+04	0.0	0.0	0.0	0.0	0.0	-0.2874E-03	0.3700E-01	0.7260E+00	-0.3623E+00	0.7258E+00	-0.3253E+00
0.2000E+04	0.0	0.0	0.0	0.0	0.0	-0.1230E-01	0.3980E-01	0.7816E+00	-0.3269E+00	0.7693E+00	-0.2871E+00
0.1500E+04	0.0	0.0	0.0	0.0	0.0	-0.2732E-01	0.3758E-01	0.8399E+00	-0.2799E+00	0.8126E+00	-0.2423E+00
0.1000E+04	0.0	0.0	0.0	0.0	0.0	-0.4299E-01	0.2659E-01	0.8995E+00	-0.2170E+00	0.8565E+00	-0.1904E+00
0.5000E+03	0.0	0.0	0.0	0.0	0.0	-0.5015E-01	0.2243E-02	0.9574E+00	-0.1306E+00	0.9073E+00	-0.1284E+00
0.2500E+03	0.0	0.0	0.0	0.0	0.0	-0.4094E-01	-0.1398E-01	0.9829E+00	-0.7385E-01	0.9420E+00	-0.8783E-01
0.1000E+03	0.0	0.0	0.0	0.0	0.0	-0.2258E-01	-0.1972E-01	0.9952E+00	-0.3273E-01	0.9726E+00	-0.5245E-01
0.5000E+02	0.0	0.0	0.0	0.0	0.0	-0.1140E-01	-0.1636E-01	0.9982E+00	-0.1719E-01	0.9868E+00	-0.3355E-01
0.2500E+02	0.0	0.0	0.0	0.0	0.0	-0.4806E-02	-0.1102E-01	0.9993E+00	-0.8892E-02	0.9945E+00	-0.1991E-01
0.1000E+02	0.0	0.0	0.0	0.0	0.0	-0.1227E-02	-0.5370E-02	0.9998E+00	-0.3662E-02	0.9986E+00	-0.9032E-02

CENTRAL LOOP H-FIELDS (NSTYP = 4), NORMALIZED BY H-FS

NFREQ = 10 NLYR = 3 NSRC = 1 NLPSEP = 1

FREQ(I): 0.2500E+04 0.2000E+04 0.1500E+04 0.1000E+04 0.5000E+03 0.2500E+03 0.1000E+03 0.5000E+02 0.2500E+02 0.1000

DEPL(I): 100.00 300.00

RHOL(I): 100.00 10.00 100.00

LOOP SIDE LENGTH IS 250.0 M, PROFILE AZIMUTH IS 90.

SOURCE CENTER POSITIONS ----- (X,Y,Z)

0.00 0.00

RECEIVER POSITIONS W.R.T. SOURCE CENTER

0.00 0.00

FREQ	XSRC	YSRC	XREC	YREC	ZREC	HZSN (Re,Im)		HZON (Re,Im)		HZT (Re,Im)	
0.2500E+04	0.0	0.0	0.0	0.0	0.0	0.0000E+00	0.0000E+00	0.7150E+00	-0.3183E+00	0.7150E+00	-0.3183E+00
0.2000E+04	0.0	0.0	0.0	0.0	0.0	0.0000E+00	0.0000E+00	0.7577E+00	-0.2828E+00	0.7577E+00	-0.2828E+00
0.1500E+04	0.0	0.0	0.0	0.0	0.0	0.0000E+00	0.0000E+00	0.8009E+00	-0.2409E+00	0.8009E+00	-0.2409E+00
0.1000E+04	0.0	0.0	0.0	0.0	0.0	0.0000E+00	0.0000E+00	0.8461E+00	-0.1916E+00	0.8461E+00	-0.1916E+00
0.5000E+03	0.0	0.0	0.0	0.0	0.0	0.0000E+00	0.0000E+00	0.8995E+00	-0.1316E+00	0.8995E+00	-0.1316E+00
0.2500E+03	0.0	0.0	0.0	0.0	0.0	0.0000E+00	0.0000E+00	0.9366E+00	-0.9133E-01	0.9366E+00	-0.9133E-01
0.1000E+03	0.0	0.0	0.0	0.0	0.0	0.0000E+00	0.0000E+00	0.9695E+00	-0.5551E-01	0.9695E+00	-0.5551E-01
0.5000E+02	0.0	0.0	0.0	0.0	0.0	0.0000E+00	0.0000E+00	0.9851E+00	-0.3600E-01	0.9851E+00	-0.3600E-01
0.2500E+02	0.0	0.0	0.0	0.0	0.0	0.0000E+00	0.0000E+00	0.9938E+00	-0.2159E-01	0.9938E+00	-0.2159E-01
0.1000E+02	0.0	0.0	0.0	0.0	0.0	0.0000E+00	0.0000E+00	0.9984E+00	-0.9852E-02	0.9984E+00	-0.9852E-02

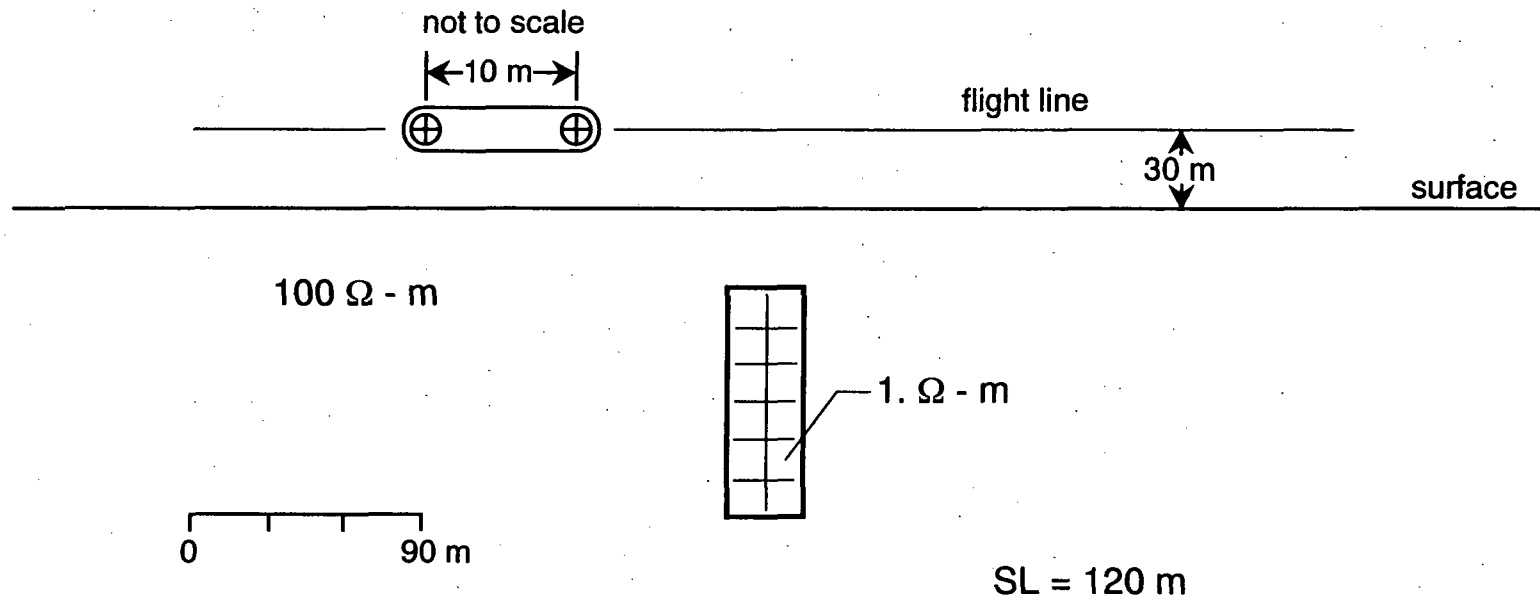


Figure A-5. Buried conductive prism (1. ohm-m) in a resistive half-space simulated for airborne loop-loop arrays. The structure has two planes of symmetry with 24 cells per quadrant. Two loop modes, HCP and VCA, at a height of 30 m and a source-receiver separation of 10 m are considered. Secondary vertical magnetic fields normalized by the free-space results are computed every 25 m across the center of the prism at a frequency of 1000 Hz.

6,1,1,1  
1000.  
100.  
19,1,25.,90.,1  
0.,-5.,-30.,2  
0.,10.  
1,6,2,0.,0.  
1.  
15.,37.5,4,1  
15.,15.,15.,15.  
15.  
1111  
15.,52.5,4,1  
15.,15.,15.,15.  
15.  
1111  
15.,67.5,4,1  
15.,15.,15.,15.  
15.  
1111  
15.,82.5,4,1  
15.,15.,15.,15.  
15.  
1111  
15.,97.5,4,1  
15.,15.,15.,15.  
15.  
1111  
15.,112.5,4,1  
15.,15.,15.,15.  
15.  
1111

SLINGRAM LOOP H-FIELDS (NSTYP = 6), NORMALIZED BY H-FS

NFREQ = 1 NLYR = 1 NSRC = 19 NLPSEP = 1

FREQ(I): 0.1000E+04

RHOL(I): 100.00

LOOP SEPARATION IS 10.0 M, PROFILE AZIMUTH IS 90. LOOP FORMAT = 1

SOURCE LOOP POSITIONS ----- (X,Y,Z)

0.00	-230.00	-30.00	0.00	-205.00	-30.00	0.00	-180.00	-30.00
0.00	-155.00	-30.00	0.00	-130.00	-30.00	0.00	-105.00	-30.00
0.00	-80.00	-30.00	0.00	-55.00	-30.00	0.00	-30.00	-30.00
0.00	-5.00	-30.00	0.00	20.00	-30.00	0.00	45.00	-30.00
0.00	70.00	-30.00	0.00	95.00	-30.00	0.00	120.00	-30.00
0.00	145.00	-30.00	0.00	170.00	-30.00	0.00	195.00	-30.00
0.00	220.00	-30.00						

ISYM = 2 NCEL = 24 NRES = 1

FREQ	XPLT	YPLT	ZREC	HZSN (Re,Im - ppm)		HZON (Re,Im - ppm)		HZTN (Re,Im - ppm)	
0.1000E+04	0.0	-225.0	-30.0	2	0	59	221	61	221
0.1000E+04	0.0	-200.0	-30.0	2	1	59	221	61	222
0.1000E+04	0.0	-175.0	-30.0	3	2	59	221	63	223
0.1000E+04	0.0	-150.0	-30.0	5	4	59	221	64	225
0.1000E+04	0.0	-125.0	-30.0	7	7	59	221	67	228
0.1000E+04	0.0	-100.0	-30.0	11	13	59	221	70	234
0.1000E+04	0.0	-75.0	-30.0	14	21	59	221	73	242
0.1000E+04	0.0	-50.0	-30.0	16	27	59	221	75	248
0.1000E+04	0.0	-25.0	-30.0	11	22	59	221	70	243
0.1000E+04	0.0	0.0	-30.0	5	15	59	221	64	236
0.1000E+04	0.0	25.0	-30.0	11	22	59	221	70	243
0.1000E+04	0.0	50.0	-30.0	16	27	59	221	75	248
0.1000E+04	0.0	75.0	-30.0	14	21	59	221	73	242
0.1000E+04	0.0	100.0	-30.0	11	13	59	221	70	234
0.1000E+04	0.0	125.0	-30.0	7	7	59	221	67	228
0.1000E+04	0.0	150.0	-30.0	5	4	59	221	64	225
0.1000E+04	0.0	175.0	-30.0	3	2	59	221	63	223
0.1000E+04	0.0	200.0	-30.0	2	1	59	221	61	222
0.1000E+04	0.0	225.0	-30.0	2	0	59	221	61	221

SLINGRAM LOOP H-FIELDS (NSTYP = 6), NORMALIZED BY H-FS

NFREQ = 1 NLYR = 1 NSRC = 19 NLPSEP = 1

FREQ(I): 0.1000E+04

RHOL(I): 100.00

LOOP SEPARATION IS 10.0 M, PROFILE AZIMUTH IS 90. LOOP FORMAT = 2

SOURCE LOOP POSITIONS ----- (X,Y,Z)

0.00	-230.00	-30.00	0.00	-205.00	-30.00	0.00	-180.00	-30.00
0.00	-155.00	-30.00	0.00	-130.00	-30.00	0.00	-105.00	-30.00
0.00	-80.00	-30.00	0.00	-55.00	-30.00	0.00	-30.00	-30.00
0.00	-5.00	-30.00	0.00	20.00	-30.00	0.00	45.00	-30.00
0.00	70.00	-30.00	0.00	95.00	-30.00	0.00	120.00	-30.00
0.00	145.00	-30.00	0.00	170.00	-30.00	0.00	195.00	-30.00
0.00	220.00	-30.00						

ISYM = 2 NCEL = 24 NRES = 1

FREQ	XPLT	YPLT	ZREC	HYSN (Re,Im - ppm)		HYON (Re,Im - ppm)		HYTN (Re,Im - ppm)	
0.1000E+04	0.0	-225.0	-30.0	0	0	-15	-55	-15	-55
0.1000E+04	0.0	-200.0	-30.0	0	0	-15	-55	-15	-55
0.1000E+04	0.0	-175.0	-30.0	0	-1	-15	-55	-15	-55
0.1000E+04	0.0	-150.0	-30.0	0	-1	-15	-55	-15	-55
0.1000E+04	0.0	-125.0	-30.0	0	0	-15	-55	-15	-55
0.1000E+04	0.0	-100.0	-30.0	0	0	-15	-55	-15	-55
0.1000E+04	0.0	-75.0	-30.0	-1	0	-15	-55	-16	-55
0.1000E+04	0.0	-50.0	-30.0	-3	-3	-15	-55	-18	-58
0.1000E+04	0.0	-25.0	-30.0	-9	-12	-15	-55	-24	-67
0.1000E+04	0.0	0.0	-30.0	-13	-19	-15	-55	-28	-74
0.1000E+04	0.0	25.0	-30.0	-9	-12	-15	-55	-24	-67
0.1000E+04	0.0	50.0	-30.0	-3	-3	-15	-55	-18	-58
0.1000E+04	0.0	75.0	-30.0	-1	0	-15	-55	-16	-55
0.1000E+04	0.0	100.0	-30.0	0	0	-15	-55	-15	-55
0.1000E+04	0.0	125.0	-30.0	0	0	-15	-55	-15	-55
0.1000E+04	0.0	150.0	-30.0	0	-1	-15	-55	-15	-55
0.1000E+04	0.0	175.0	-30.0	0	-1	-15	-55	-15	-55
0.1000E+04	0.0	200.0	-30.0	0	0	-15	-55	-15	-55
0.1000E+04	0.0	225.0	-30.0	0	0	-15	-55	-15	-55